Fig. 1.

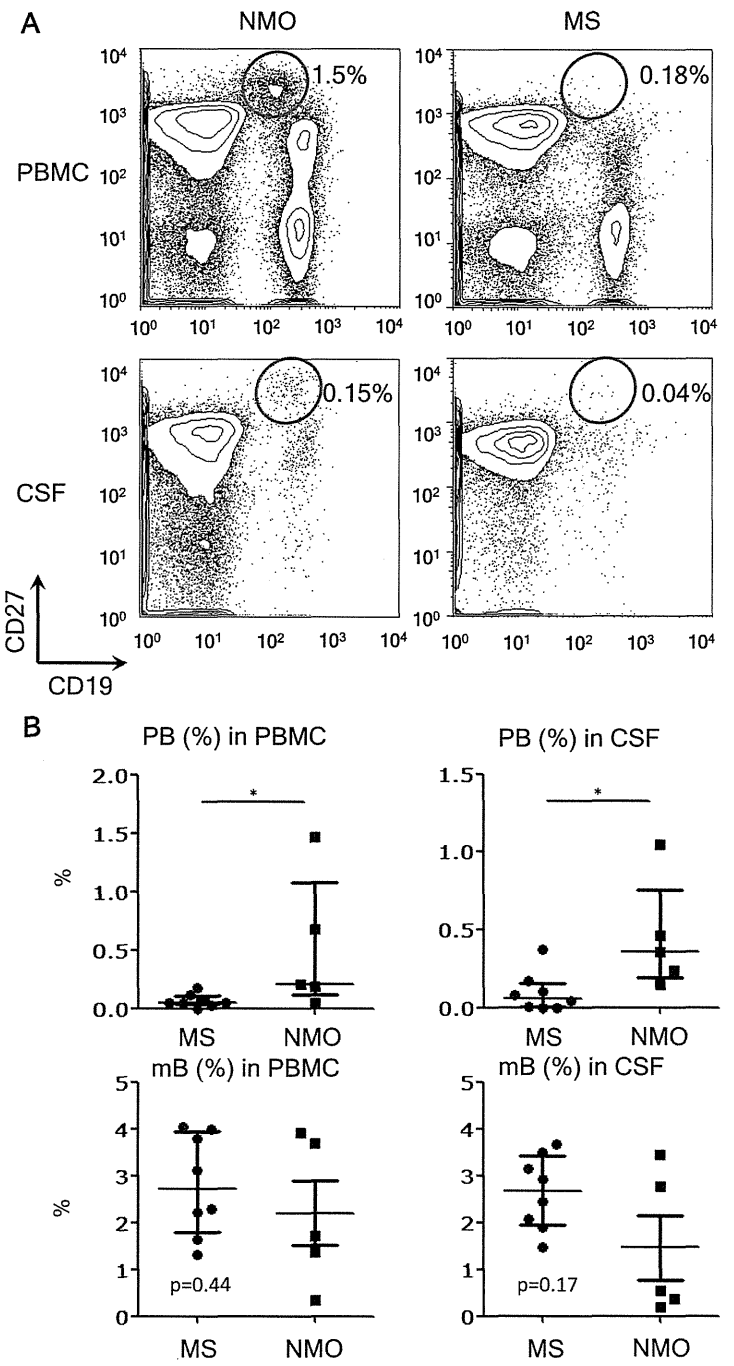

Figure 1. Selective increase of plasmablasts (PBs) during relapse of NMO. (A) B-cell subpopulation analysis by flow cytometry. Peripheral blood mononuclear cell (PBMC) and cerebrospinal fluid (CSF) cells were obtained during relapse of neuromyelitis optica (NMO) or multiple sclerosis (MS) and were stained with fluorescence-conjugated anti-CD19, -CD27, -CD38, and -CD180 monoclonal antibodies (mAbs). PB cells ($CD19^{int}CD27^{high}$) were encircled after observing that they also bear the phenotype of $CD38^{high}CD180^{-}$ (Figure S1). Values represent the percentages of PB cells among all mononuclear cells.
(B) The proportion of PB and memory B-cells (mB) in PBMC and CSF from MS and NMO during relapse. The data were obtained from eight patients with MS and five with NMO [*$p < 0.05$ by Mann–Whitney test; each error bar represents the median ± interquartile range (IQR)].

doi: 10.1371/journal.pone.0083036.g001

cell marker CD138 [12]. CD138 is known to be an adhesion molecule as well as a negative regulator of cell migration [23]. Both $CD138^+$ and $CD138^-$ PBs are able to produce AQP4-Ab [12]. However, the mutual relationship of these PB subsets remained obscure. The expression of HLA-DR was examined, because PB cells that produce IgG autoantibodies reportedly express HLA-DR [24]. We found that only the proportion of $CD138^+HLA\text{-}DR^+$ PBs significantly increased during the relapse of NMO, compared with remission (Figure **2A**). More importantly, we found that the $CD138^+HLA\text{-}DR^+$ PBs comprised the vast majority of PBs in the CSF of NMO patients in relapse (Figure **2B**). Since CD138 is thought to be upregulated in activated cells [23], we speculated that antibody-producing PB cells ($CD138^+HLA\text{-}DR^+$ PB) were activated in the periphery in the patients during relapse, and that they might preferentially be recruited to the CSF and be further activated.

$CD138^+HLA\text{-}DR^+$ PB cells represent recently differentiated IgG-producing PBs

Previous studies showed that activated PB cells secreting IgGs would increase in the peripheral blood of healthy individuals after receiving vaccination [25,26]. To strengthen our postulate that $CD138^+HLA\text{-}DR^+$ PBs are recently activated IgG-secreting PBs, we also characterized the PB phenotypes in healthy vaccinated individuals. We found that proportions of $CD138^+$ PBs, but not $CD138^-$ PBs, among $CD19^+$ B-cells significantly increased one week after influenza vaccination. Neither mB nor naïve B-cells (nB) were altered (Figure **3A**). This observation suggests that $CD138^+$ PB cells are more enriched among germinal center-derived cells than $CD138^-$ PB. Next, we compared $HLA\text{-}DR^+$ and $HLA\text{-}DR^-$ PBs from vaccinated individuals for the intracellular expression of IgGs. We confirmed that $HLA\text{-}DR^+$ PBs were the major producer of IgGs (Figure **3B**). These results support further that $CD138^+HLA\text{-}DR^+$ PBs, which increase during the relapse of NMO, correspond to recently activated IgG-producing cells.

$CD138^+HLA\text{-}DR^+$ PBs upregulate CXCR3 during relapse of NMO

Results of chemo-attractant assays showed that CXCR4 and CXCR3 ligands would attract PB cells, but not mature plasma cells [27]. The expression of CXCR4 on PB is important for their homing to the bone marrow, whereas the interaction of CXCR3 with its ligand CXCL10 plays a key role in the migration of PBs toward inflamed tissues. CXCL10 is thought to play a critical role in NMO [17]. Therefore, we analyzed the expression of CXCR4 and CXCR3 on PB cells in the peripheral blood of NMO patients. We observed that the expression levels of CXCR3 on PBs or activated PBs ($CD138^+HLA\text{-}DR^+$) were significantly higher during relapse than in remission of NMO. It appeared that the upregulation of CXCR4 on PBs during relapse was less obvious (Figure **4A**). We further analyzed the PBMC obtained during relapse and in remission for the expression of CXCR3 and CXCR4 according to B-cell subpopulations. Proportions (%) of $CXCR3^+$ cells among mB and nB cells were 17% and 2%, respectively during relapse and did not differ from remission, whereas that for PBs was approximately 50% during relapse compared to 23% in remission (Figure **4B**). In contrast, the percentages of $CXCR4^+$ cells were higher in mB and nB cells (50% and 56%, respectively) than that in PBs (15%) during relapse. These percentages of $CXCR4^+$ B-cell subpopulations did not differ from those during remission. The increased CXCR3 expression on PBs during relapse suggests biological significance and allows us to speculate that the migration of $CD138^+HLA\text{-}DR^+$ PBs to the CNS might involve a CXCR3-dependent mechanism.

Peripheral PBs and CSF PB have common IgG variable regions

Single-cell sorting of lymphocytes is a refined method for characterizing the cellular properties of human B-cell lineages [10,21,25,28]. To characterize the antibody gene repertoire of the IgG-producing PBs in patients with NMO, we performed a single-cell sorting of PB clones from peripheral blood and CSF during relapse of NMO, and sequenced the gene fragments of the heavy and light chain variable regions after cloning. In principle, B-cell V regions are rearranged within the germinal centers and acquire the ability to produce high-affinity antibodies that are diversified by somatic hypermutation. We compared these variable region sequences with the germline database of IgBLAST (www.ncbi.nlm.nih.gov/igblast/) to estimate the number of mutations. In addition, the ratio of replacement to silent mutations (R/S ratio) was analyzed in single-cell sorted PBs derived from a patient with NMO. We established 38 paired vector clones containing cDNAs of heavy- and light-chain variable regions. The variable regions of the PB IgG heavy chain contained an average of 17 mutations and had higher R/S ratios in CDRs than in framework regions (FR) (Figures **S4** and **S5**). Moreover, the variable regions of the IgG κ chains of the sorted PB contained an average of 10 mutations and also had higher R/S ratios in CDRs than in FR. However, there were no significant differences in the number of mutations between the PB clones from peripheral blood and from CSF (Figure **S6**). The numbers of mutations in these PB clones did not differ from those in IgG^+ mB [28]. These results confirmed that PB clones derived from NMO would represent a post-germinal center B-cell lineage.

The similarity in the numbers of mutations in peripheral and CSF PB clones prompted us to address whether differentiated PBs might migrate from peripheral blood to CSF without further affinity maturation. Therefore, we compared the sequences of the CDR regions of PB clones from peripheral blood and CSF. Single-cell sorted PBs (109 from peripheral blood and 67 from CSF) were obtained from two patients with NMO in relapse. Because our target was recently differentiated PB derived from germinal centers, we selectively amplified the CDR3 regions of the IgG H-chains. The CDR3 regions of the IgG genes (41 from patient 1 and 51 from patient 2) were successfully sequenced. The clones were numbered in the order they were collected. We noticed that 11 CDR3 sequences were repeatedly detected in 17 CSF PB clones and 21 peripheral blood PB clones (Table **2**). Interestingly, five of the 11 sequences were detected in both peripheral blood and CSF clones of the same patient (clone numbers in bold), indicating the migration of the PB clones from the peripheral blood to the CSF. Interestingly, a common

Fig. 2.

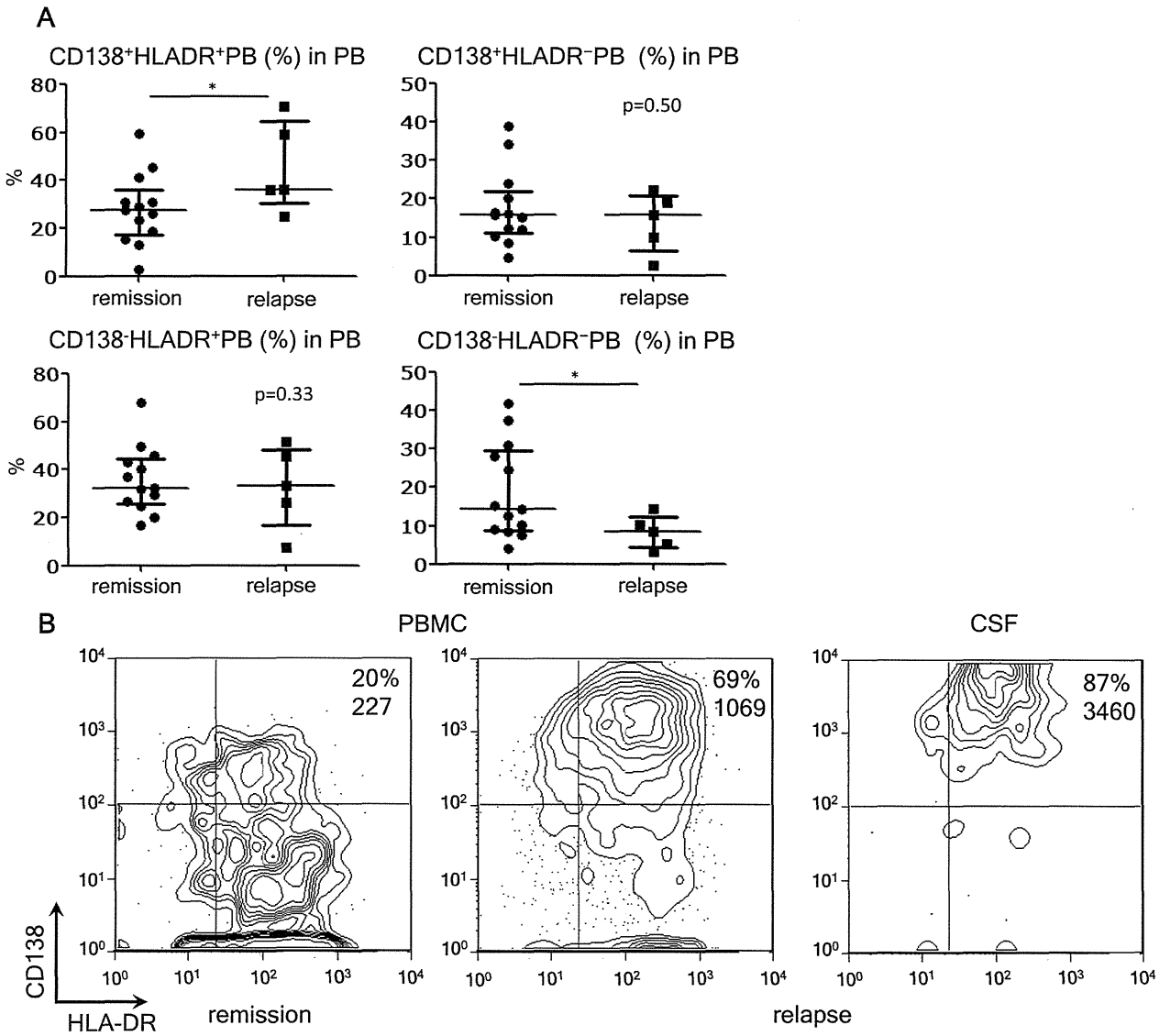

Figure 2. Kinetics of CD138⁺HLA-DR⁺ PB during relapse of NMO. (A) Analysis of pooled peripheral blood mononuclear cells (PBMC) data from neuromyelitis optica (NMO) in remission and relapse. The plasmablasts (PBs) were subdivided into four subpopulations by considering the expression of CD138 and HLA-DR. The individual data show the percentages of each PB subpopulation among the total PB [*$p < 0.05$ by Mann–Whitney test; each error bar represents the median ± interquartile range (IQR)].

(B) Enrichment of CD138⁺HLA-DR⁺ PBs in the CSF. The PBMC and CSF cells were obtained from NMO during relapse. The values indicate the percentages of CD138⁺HLA-DR⁺ PBs among the total PB. The expression level of CD138 was assessed by mean fluorescence intensity (MFI). Representative data of one out of three different cases are shown.

doi: 10.1371/journal.pone.0083036.g002

CDR3 sequence (VKFSATAAAGNWDHFDY) was obtained from the PB clones from both patients (peripheral blood-derived clones 28 and 30 and CSF-derived clone 36 in patient 1; peripheral clones 3 and 24 and CSF-derived clones 1, 2, and 22 in patient 2 with the CDR3 sequence). These results suggested that the PBs seem to be inclined toward several representative clones during the relapse of NMO. Although the pathological implications remain obscure, it might be important to follow up in a larger patient cohort.

Fig. 3.

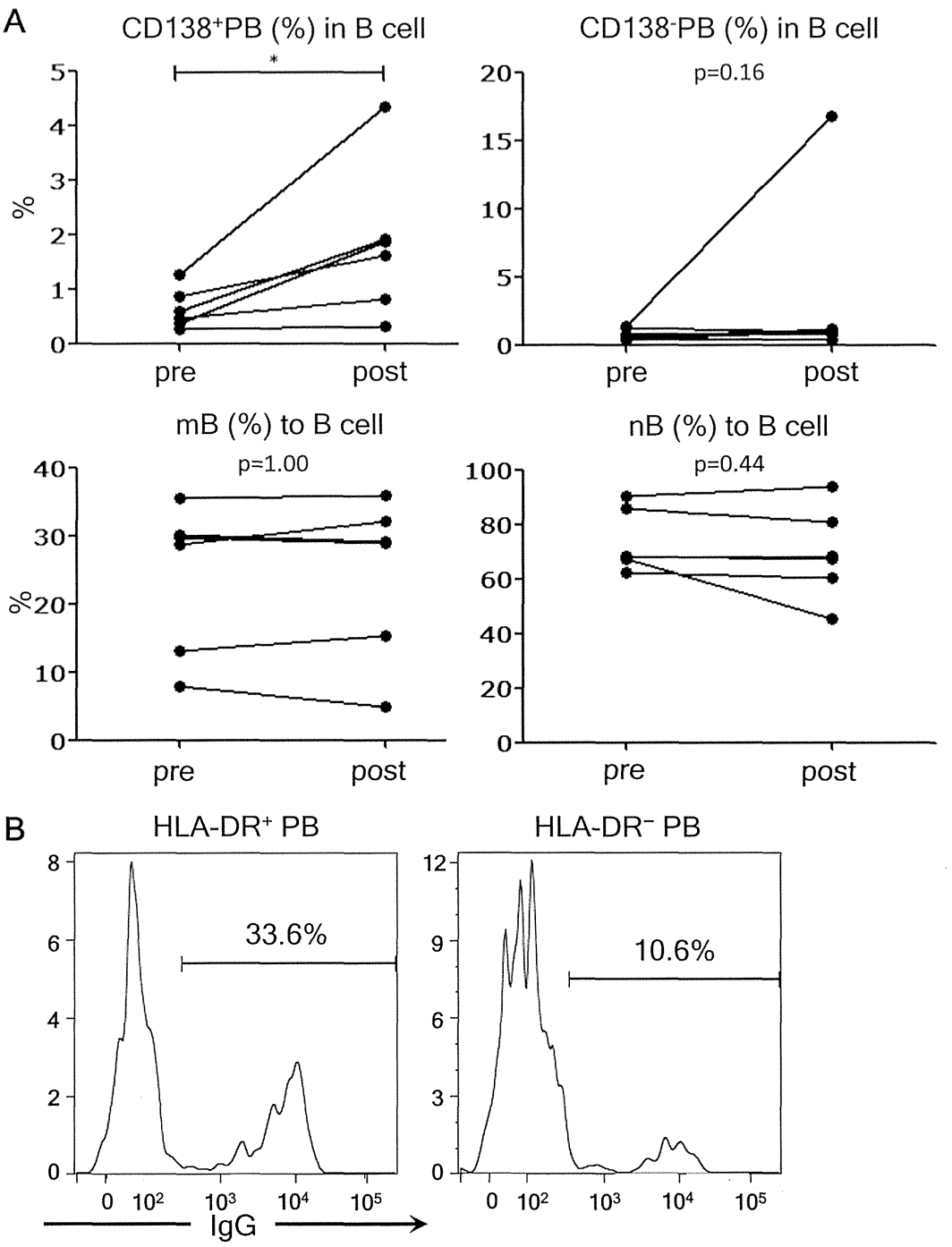

Figure 3. CD138⁺HLA-DR⁺ plasmablasts (PB) cells are recently differentiated IgG-producing PB. (A) The effects of influenza vaccination on the frequencies of B-cell subpopulations were analyzed. The frequency of each B-cell subpopulation derived from the peripheral blood of healthy subjects before (pre) and seven days after vaccination (post) is shown. Each line connects the values obtained from a single subject (*$p < 0.05$ by Wilcoxon signed rank test).
(B) The results of intracellular IgG staining of HLA-DR⁺ PB (left) and HLA-DR⁻ PBs (right) are shown. The values represent the percentages of IgG-producing cells in each PB subpopulation. Representative data of one out of three individuals are displayed.
doi: 10.1371/journal.pone.0083036.g003

Fig. 4.

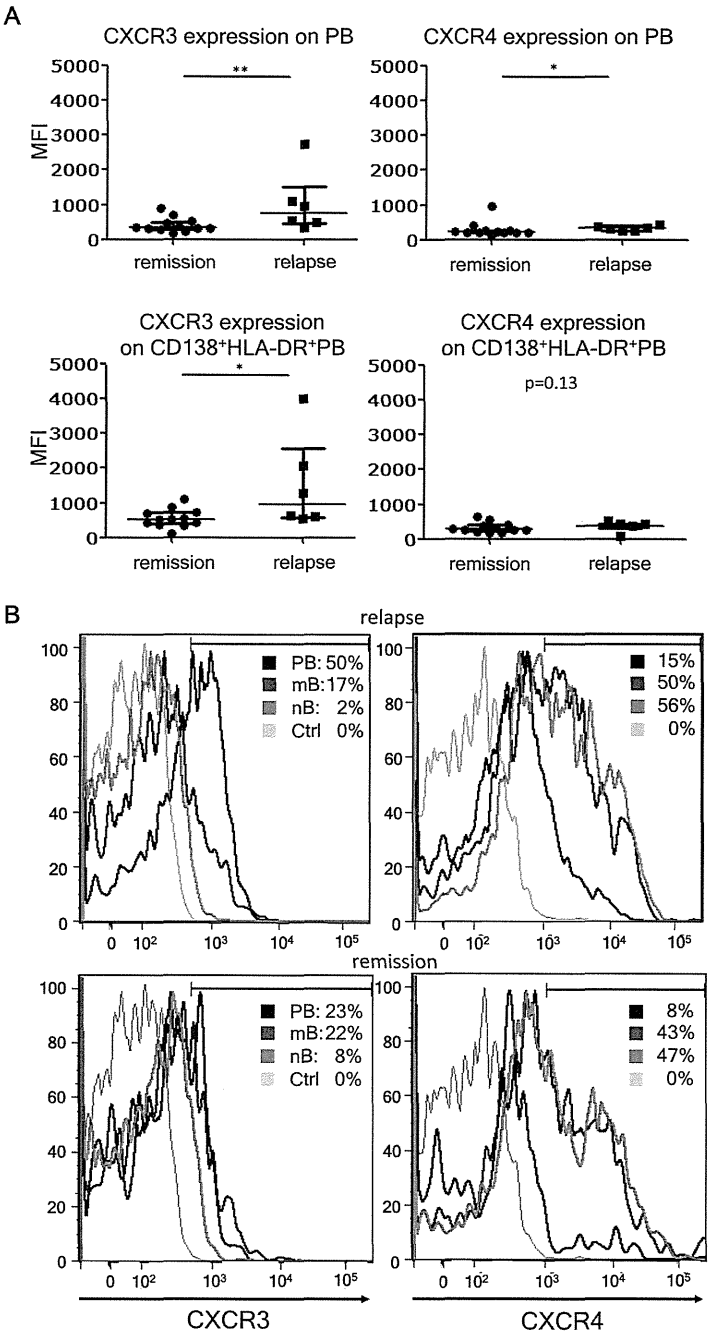

Figure 4. CXCR3 expression on plasmablasts (PBs) correlates with the disease state. (A) CXCR3 and CXCR4 on PB in neuromyelitis optica (NMO) relapse and remission. Here, we compared the mean fluorescence intensity (MFI) of CXCR3 and CXCR4 expression in the peripheral blood PBs during remission and relapse of NMO. MFI of CXCR3 and CXCR4 expressions on $CD138^+HLA\text{-}DR^+$ PBs were also analyzed [$^{**}p < 0.01$ and $^{*}p < 0.05$ by Mann–Whitney test; each error bar represents the median ± interquartile range (IQR]].

(B) B-cell subpopulations derived from peripheral blood mononuclear cells (PBMC) during disease relapse and remission were analyzed by flow cytometry to investigate the expression of CXCR3 and CXCR4. The values represent the percentages of $CXCR3^+$ or $CXCR4^+$ cells within each B-cell subpopulation. Unstained control of PBMC is indicated by Ctrl. Representative data of at least five patients in each disease state are shown.

doi: 10.1371/journal.pone.0083036.g004

Table 2. V_H sequences of the plasmablasts (PBs) clones.

Clones derived from peripheral blood	Clones derived from the cerebrospinal fluid (CSF)	H chain of CDR3	Germline	Joint region
pt1-**28, 30**	**36**	VKFSATAAAGNWDHFDY	VH3-23	J4
pt1-**26**	**12, 15**	ARGFYYGSGSRRGMDV	VH4-4	J6
pt1-22, 23	—	ARGDNGSFSY	VH3-74	J4
pt1-□	8, 13	ARGIVTA	VH3-7	J4
pt1-□	34, 39	ARQATEQVPVLPFVMGAPRKKGGAFNV	VH4-39	J4
pt2-33, 37, 39	—	VRDSPPPATHFDY	VH3-21	J4
pt2-**27**	**25, 30, 32, 35, 36, 40**	ARMARAGNYANNWYDP	VH4-59	J4
pt2-**3, 24**	**1, 2, 22**	VKFSATAAAGNWDHFDY	VH3-23	J4
pt2-**4, 6, 10, 12, 13, 20**	**8**	AREDLPGTMFDY	VH3-33	J4
pt2-23, 26	—	VRDNWGVDY	VH3-74	J4
pt2-21, 31	—	RCHRDRSGSPVGWYAP	VH4-30	J4

The IgG heavy chain sequences in the PB clones from neuromyelitis optica (NMO) patients were determined. Distinct PB clones obtained from peripheral blood and CSF samples are numbered in the order they were collected. In the table are shown the amino acid sequences of 11 CDR3 that were repeatedly detected in the PB clones, V_H gene (germline), and joint regions. When the same sequences were detected in both peripheral blood and CSF clones of the same patient, the clone numbers were highlighted in bold.

doi: 10.1371/journal.pone.0083036.t002

Discussion

NMO is an inflammatory disease with a pathology characterized by AQP4-Ab–mediated astrocytopathy in the CNS lesions. As previously reported, IL-6 as well as IL-6-dependent PBs, a terminally differentiated B-cell population, are involved in the pathogenesis [12]. Results of laboratory works have suggested that the AQP4-Ab produced in the periphery might cause the astrocyte pathology [9–11], assuming that they could enter the CNS through the disrupted area of the BBB. However, the role of antibody production within the CNS has not been excluded in human NMO. In fact, it remains unclear why AQP4-expressing organs, including kidney and stomach, are not involved in NMO, despite the presence of AQP4-Abs in the periphery [29]. It is unknown whether PBs play a pathogenic role within the CNS after migrating to the CNS. Here, we demonstrated that CSF lymphocytes from NMO during relapse are enriched in activated PB cells, brightly expressing CD138 and HLA-DR. CD138 serves not only as a negative regulator of cell migration in vitro [23], but also as the marker of tissue migrating plasmablasts/plasma cells in vivo [27]. We have confirmed that HLA-DR expression would characterize the PB subset capable of secreting IgG in healthy vaccinated subjects (Figure **3B**). It is possible that the increased frequency of HLA-DR$^+$ PBs in NMO reflects an antigen-driven B-cell activation that plays a key role in NMO pathogenicity. Moreover, we showed that the CD138$^+$HLA-DR$^+$ PBs would selectively upregulate CXCR3 during relapse. Because CXCL10, a CXCR3 ligand, is present in the CSF of NMO [17], we speculate that the activated PBs might migrate from the periphery to the CNS in a CXCR3-dependent manner. Intriguingly, a study on a neurotropic coronavirus-induced encephalomyelitis model showed that CXCR3-expressing PBs would infiltrate the CNS and locally produce antibodies against the pathogen [30]. The viral encephalomyelitis induced in CXCR3-knockout mice was remarkably exacerbated in association with a marked reduction of PB cells infiltration. Although this work highlights the importance of CXCR3-dependent PB migration in the production of antiviral antibodies within the CNS, it also gives us a clue to understand how migratory PBs would contribute to the pathogenesis of NMO.

We further proved that IgG-producing PBs in the CSF during relapse share identical CDR sequences with those from PBs in the peripheral blood (Table **2**). The IgG sequences were highly mutated (Figure **S4** and **S5**), indicating that helper T-cells guided the PBs toward germinal centers. Although we did not separate CD138$^-$ and CD138$^+$ PBs in this analysis, the number of mutations in the H-chain variable regions showed a single-peak distribution (Figure **S4**). These results suggest that both CD138$^-$ and CD138$^+$ PBs are affinity-maturated B-cells, although CD138 expression levels could inversely correlate with the tissue-migrating ability [23]. There remained a possibility that mB might give rise to PBs within the CSF. However, further affinity maturation in PBs was not observed in CSF compared with peripheral blood, indicating that clonal expansion and differentiation of mB in the CSF is not a major pathway. This assumption is also supported by the rare occurrence of CSF oligoclonal bands and raised IgG index in NMO, which indicates that the intrathecal IgG synthesis was low, transient, and restricted to acute relapse in NMO patients [6,31]. Taken together, it is likely that CXCR3-expressing PBs are expanded in the periphery and recruited to the CNS in the pathogenesis of NMO. In the CNS, B-cell stimulatory cytokines such as IL-6 would support the PB survival and AQP4-Ab production, leading to the destruction of astrocytes and the glia limitans. We and another group have shown that PBs from peripheral blood and CSF produce anti-AQP4 IgG antibody in NMO [10,12]. We therefore postulated that the common IgGs shared by PBs from the PBMC and CSF (Table 2) could bind to AQP4. Despite substantial efforts, however, we have not succeeded in this attempt so far. Though we speculate that peripherally expanded PBs producing anti-AQP4 should be able to cross BBB like other PBs, irrespective of the antigen

specificity, more efforts will be needed to formally prove our postulate.

We previously demonstrated the role of IL-6-dependent PBs in the production of AQP4-Ab [12]. In the present report, we indicate that PBs may play a more critical role in the CNS by locally producing AQP4-Ab. The relevance of this model can be verified in clinical trials of drugs targeting appropriate cells or molecules. In fact, we have recently shown that humanized anti–IL-6 receptor antibody (Tocilizumab) was efficacious in a patient with NMO in reducing the number of PBs in the peripheral blood as well as stabilizing the clinical conditions [32]. In another report, Tocilizumab successfully controlled three NMO patients who were resistant to the anti-CD20 antibody Rituximab [33]. These results indicate that PBs, rather than $CD20^+$ mB, play a pivotal role in NMO. Therefore, it will be intriguing to test the effect of drugs altering the migration of PBs toward the CNS [34].

Supporting Information

Figure S1. Flow cytometric analysis of PB. Flow cytometric scheme of B-cell subpopulation analysis. The partitioned cells are $CD19^+CD27^+$ cells within peripheral blood mononuclear cells (PBMC; left panel). The $CD19^+CD27^+$ cells were further analyzed to investigate the expression of CD38 and CD180 (middle panel). $CD38^{high}CD180^-$ cells (partitioned in the middle panel), corresponding to plasmablast (PB) cells, were analyzed again to investigate the expression of CD19 and CD27 (right panel). This result assured that the encircled population in Figure 1A represented $CD19^{int}CD27^{high}CD38^{high}CD180^-$ PB cells.
(TIF)

Figure S2. B-cell proportions in peripheral blood mononuclear cells (PBMC) and cerebrospinal fluid (CSF) from NMO and MS. PBMC and CSF were obtained from neuromyelitis optica (NMO) and multiple sclerosis (MS) patients. Here, we show the proportions (%) of total B-cells ($CD19^+$) and $CD19^+CD27^+$ cells among the PBMC and CSF. The Mann-Whitney test provided the statistical p values. The bars represent the median ± interquartile range (IQR).
(TIF)

Figure S3. The proportion of plasmablast (PB) cells among the total B-cells. Peripheral blood mononuclear cells (PBMC) and cerebrospinal fluid (CSF) were obtained from neuromyelitis optica (NMO) and multiple sclerosis (MS) patients. The proportions (%) of PB cells among the total B cells ($CD19^+$) are reported. The Mann-Whitney test provided the statistical p values (**$p < 0.01$; *$p < 0.05$). The bars represent the median ± interquartile range (IQR).
(TIF)

Figure S4. The number of somatic hypermutations in plasmablast (PB) clones. V_H and V_{Kappa} regions of the IgG gene were evaluated in a total of 38 PB clones derived from a patient with neuromyelitis optica NMO (Pt1) during relapse. There were 17.4 ± 1.3 [mean ± standard error of the mean (SEM)] in the V_H regions and 10.5 ± 1.5 mutations in the V kappa regions.
(TIF)

Figure S5. Plasmablast (PB) cells are diversified by somatic hypermutations. The mutation frequencies in the framework regions (FR) and in complementarity-determining regions (CDR) of the V_H and V_{Kappa} regions of the IgG genes were analyzed in PB clones from patient 1 (Pt1). The ratio of replacement (R, black bars) to silent (S, white bars) changes are shown at the bottom (R/S ratio).
(TIF)

Figure S6. Comparison of the somatic hypermutations in peripheral blood mononuclear cells (PBMC)- and cerebrospinal fluid (CSF)-derived PB clones. Here, we compare the plasmablast (PB) clones derived from the peripheral blood (N = 14) and from CSF (N = 24) with the number of mutations in the V_H and V_{Kappa} regions of the IgG genes. The statistic p values were obtained by Mann-Whitney test. The data represent the median ± interquartile range (IQR).
(TIF)

Acknowledgements

We thank Dr. Toshiyuki Takahashi and Dr. Kazuo Fujihara (Tohoku University) for performing the assays of AQP4-Ab detection.

Author Contributions

Conceived and designed the experiments: NC TA SO SM TY. Performed the experiments: NC TM. Analyzed the data: NC TA TM MN TY. Contributed reagents/materials/analysis tools: HK KY YK NH TO MM TT. Wrote the manuscript: NC TA TY. Supervised the work: TY.

References

1. Wingerchuk DM, Hogancamp WF, O'Brien PC, Weinshenker BG (1999) The clinical course of neuromyelitis optica (Devic's syndrome). Neurology 53: 1107-1114. doi:10.1212/WNL.53.5.1107. PubMed: 10496275.
2. Lennon VA, Wingerchuk DM, Kryzer TJ, Pittock SJ, Lucchinetti CF et al. (2004) A serum autoantibody marker of neuromyelitis optica: distinction from multiple sclerosis. Lancet 364: 2106-2112. doi:10.1016/S0140-6736(04)17551-X. PubMed: 15589308.
3. Wingerchuk DM, Lennon VA, Lucchinetti CF, Pittock SJ, Weinshenker BG (2007) The spectrum of neuromyelitis optica. Lancet Neurol 6: 805-815. doi:10.1016/S1474-4422(07)70216-8. PubMed: 17706564.
4. Warabi Y, Matsumoto Y, Hayashi H (2007) Interferon beta-1b exacerbates multiple sclerosis with severe optic nerve and spinal cord demyelination. J Neurol Sci 252: 57-61. doi:10.1016/j.jns.2006.10.008. PubMed: 17125797.
5. Kleiter I, Hellwig K, Berthele A, Kümpfel T, Linker RA et al. (2012) Neuromyelitis Optica Study Group. Failure of natalizumab to prevent relapses in neuromyelitis optica. Arch Neurol 69: 239-245. doi:10.1001/archneurol.2011.216. PubMed: 22332191.
6. Misu T, Fujihara K, Kakita A, Konno H, Nakamura M et al. (2007) Loss of aquaporin 4 in lesions of neuromyelitis optica: distinction from

multiple sclerosis. Brain 130: 1224-1234. doi:10.1093/brain/awm047. PubMed: 17405762.
7. Roemer SF, Parisi JE, Lennon VA, Benarroch EE, Lassmann H et al. (2007) Pattern-specific loss of aquaporin-4 immunoreactivity distinguishes neuromyelitis optica from multiple sclerosis. Brain 130: 1194-1205. doi:10.1093/brain/awl371. PubMed: 17282996.
8. Takano R, Misu T, Takahashi T, Sato S, Fujihara K et al. (2010) Astrocytic damage is far more severe than demyelination in NMO: a clinical CSF biomarker study. Neurology 75: 208-216. doi:10.1212/WNL.0b013e3181e2414b. PubMed: 20644148.
9. Bradl M, Misu T, Takahashi T, Watanabe M, Mader S et al. (2009) Neuromyelitis optica: pathogenicity of patient immunoglobulin in vivo. Ann Neurol 66: 630-643. doi:10.1002/ana.21837. PubMed: 19937948.
10. Bennett JL, Lam C, Kalluri SR, Saikali P, Bautista K et al. (2009) Intrathecal pathogenic anti-aquaporin-4 antibodies in early neuromyelitis optica. Ann Neurol 66: 617-629. doi:10.1002/ana.21802. PubMed: 19938104.
11. Saadoun S, Waters P, Bell A, Vincent A, Verkman AS et al. (2010) Papadopoulos MC. Intra-cerebral injection of neuromyelitis optica immunoglobulin G and human complement produces neuromyelitis optica lesions in mice. Brain 133: 349-361. doi:10.1093/brain/awp309. PubMed: 20047900.
12. Chihara N, Aranami T, Sato W, Miyazaki Y, Miyake S et al. (2011) Interleukin 6 signaling promotes anti-aquaporin 4 autoantibody production from plasmablasts in neuromyelitis optica. Proc Natl Acad Sci U S A 108: 3701-3706. doi:10.1073/pnas.1017385108. PubMed: 21321193.
13. Hoyer BF, Moser K, Hauser AE, Peddinghaus A, Voigt C et al. (2004) Short-lived plasmablasts and long-lived plasma cells contribute to chronic humoral autoimmunity in NZB/W mice. J Exp Med 199: 1577-1584. doi:10.1084/jem.20040168. PubMed: 15173206.
14. Takahashi T, Fujihara K, Nakashima I, Misu T, Miyazawa I et al. (2007) Anti-aquaporin-4 antibody is involved in the pathogenesis of NMO: a study on antibody titre. Brain 130: 1235-1243. doi:10.1093/brain/awm062. PubMed: 17449477.
15. Okada K, Matsushita T, Kira J, Tsuji S (2010) B-cell activating factor of the TNF family is upregulated in neuromyelitis optica. Neurology 74: 177-178. doi:10.1212/WNL.0b013e3181c919ee. PubMed: 20065253.
16. Uzawa A, Mori M, Arai K, Sato Y, Hayakawa S et al. (2010) Cytokine and chemokine profiles in neuromyelitis optica: significance of inyterleukin-6. Mult Scler 16: 1443-1452. doi: 10.1177/1352458510379247. PubMed: 20739337.
17. Narikawa K, Misu T, Fujihara K, Nakashima I, Sato S et al. (2004) CSF chemokine levels in relapsing neuromyelitis optica and multiple sclerosis. J Neuroimmunol 149: 182-186. doi:10.1016/j.jneuroim.2003.12.010. PubMed: 15020078.
18. Wingerchuk DM, Lennon VA, Pittock SJ, Lucchinetti CF, Weinshenker BG. (2006) (2006) Revised diagnostic criteria for neuromyelitis optica. Neurology 66: 1485-1489. doi:10.1212/01.wnl.0000216139.44259.74. PubMed: 16717206.
19. Polman CH, Reingold SC, Banwell B, Clanet M, Cohen JA et al. (2011) Diagnostic criteria for multiple sclerosis: 2010 revisions to the McDonald criteria. Ann Neurol 69: 292-302. doi:10.1002/ana.22366. PubMed: 21387374.
20. Mei HE, Yoshida T, Sime W, Hiepe F, Thiele K et al. (2009) Blood-borne human plasma cells in steady state are derived from mucosal immune responses. Blood 113: 2461-2469. doi:10.1182/blood-2008-04-153544. PubMed: 18987362.
21. Tiller T, Meffre E, Yurasov S, Tsuiji M, Nussenzweig MC et al. (2008) Efficient generation of monoclonal antibodies from single human B cells by single cell RT-PCR and expression vector cloning. J Immunol Methods 329: 112-124. doi:10.1016/j.jim.2007.09.017. PubMed: 17996249.
22. Klein U, Rajewsky K, Küppers R (1998) Human immunoglobulin (Ig)M +IgD+ peripheral blood B cells expressing the CD27 cell surface antigen carry somatically mutated variable region genes: CD27 as a general marker for somatically mutated (memory) B cells. J Exp Med 188: 1679-1689. doi:10.1084/jem.188.9.1679. PubMed: 9802980.
23. Liebersbach BF, Sanderson RD (1994) Expression of syndecan-1 inhibits cell invasion into type I collagen. J Biol Chem 269: 20013-20019. PubMed: 8051085.
24. Jacobi AM, Mei H, Hoyer BF, Mumtaz IM, Thiele K et al. (2010) HLA-DR^{high}/CD27^{high} plasmablasts indicate active disease in patients with systemic lupus erythematosus. Ann Rheum Dis 69: 305-308. doi: 10.1136/ard.2008.096495. PubMed: 19196727.
25. Wrammert J, Smith K, Miller J, Langley WA, Kokko K et al. (2008) Rapid cloning of high-affinity human monoclonal antibodies against influenza virus. Nature 453: 667-671. doi:10.1038/nature06890. PubMed: 18449194.
26. Odendahl M, Mei H, Hoyer BF, Jacobi AM, Hansen A et al. (2005) Generation of migratory antigen-specific plasma blasts and mobilization of resident plasma cells in a secondly immune response. Blood 105: 1614-1620. doi:10.1182/blood-2004-07-2507. PubMed: 15507523.
27. Manz RA, Hauser AE, Hiepe F, Radbruch A (2005) Maintenance of serum antibody levels. Annu Rev Immunol 23: 367-386. doi:10.1146/annurev.immunol.23.021704.115723. PubMed: 15771575.
28. Tiller T, Tsuiji M, Yurasov S, Velinzon K, Nussenzweig MC et al. (2007) Autoreactivity in human IgG+ memory B cells. Immunity 26: 205-213. doi:10.1016/j.immuni.2007.01.009. PubMed: 17306569.
29. Ratelade J, Bennett JL, Verkman AS (2011) Intravenous neuromyelitis optica autoantibody in mice targets aquaporin-4 in peripheral organs and area postrema. PLOS ONE 6: e27412. doi:10.1371/journal.pone.0027412. PubMed: 22076159.
30. Marques CP, Kapil P, Hinton DR, Hindinger C, Nutt SL et al. (2011) CXCR3-dependent plasma blast migration to the central nervous system during viral encephalomyelitis. J Virol 85: 6136-6147. doi: 10.1128/JVI.00202-11. PubMed: 21507985.
31. Jarius S, Paul F, Franciotta D, Ruprecht K, Ringelstein M et al. (2011) Crebrospinal fluid findings in aquaporin-4 antibody positive neuromyelitis optica: reaults from 211 lumbar punctures. J Neurol Sci 306: 82-90. doi:10.1016/j.jns.2011.03.038. PubMed: 21550068.
32. Araki M, Aranami T, Matsuoka T, Nakamura M, Miyake S et al. (2013) Clinical improvement in a patient with neuromyelitis optica following therapy with the anti-IL-6 receptor monoclonal antibody tocilizumab. Mod Rheumatol 23: 827-831. doi:10.1007/s10165-012-0715-9. PubMed: 22782533.
33. Ayzenberg I, Kleiter I, Schröder A, Hellwig K, Chan A et al. (2013) Interleukin-6 receptor blockade in neuromyelitis optica patients non-responsive to anti-CD20 therapy. JAMA Neurol 70: 394-397. doi: 10.1001/jamaneurol.2013.1246. PubMed: 23358868.
34. Jenh CH, Cox MA, Reich EP, Sullivan L, Chen SC et al. (2012) A selective and potent CXCR3 antagonist SCH 546738 attenuates the development of autoimmune diseases and delays graft rejection. BMC Immunol 13: 2. doi:10.1186/1471-2172-13-2. PubMed: 22233170.

OPEN ACCESS Freely available online

PLOS | ONE

A Trifluoromethyl Analogue of Celecoxib Exerts Beneficial Effects in Neuroinflammation

Alessandra Di Penta[1,2☯], Asako Chiba[3,4☯], Iraide Alloza[1,2,5], Ane Wyssenbach[6], Takashi Yamamura[3], Pablo Villoslada[7], Sachiko Miyake[3,4], Koen Vandenbroeck[1,2,5*]

1 Neurogenomiks Laboratory, University of Basque Country (UPV/ EHU), Zamudio, Spain, **2** Achucarro Basque Center for Neuroscience, Zamudio, Spain, **3** Department of Immunology, National Institute of Neuroscience, National Center of Neurology and Psychiatry, Tokyo, Japan, **4** Department of Immunology, Juntendo University School of Medicine, Tokyo, Japan, **5** IKERBASQUE, Basque Foundation for Science, Bilbao, Spain, **6** Neurotek Laboratory, University of Basque Country (UPV/EHU), Zamudio, Spain, **7** Center of Neuroimmunology, Institute of Biomedical Research August Pi Sunyer (IDIBAPS) – Hospital Clinic of Barcelona, Barcelona, Spain

Abstract

Celecoxib is a selective cyclooxygenase-2 (COX2) inhibitor. We have previously shown that celecoxib inhibits experimental autoimmune encephalomyelitis (EAE) in COX-2-deficient mice, suggestive for a mode of action involving COX2-independent pathways. In the present study, we tested the effect of a trifluoromethyl analogue of celecoxib (TFM-C) with 205-fold lower COX-2 inhibitory activity in two models of neuroinflammation, i.e. cerebellar organotypic cultures challenged with LPS and the EAE mouse model for multiple sclerosis. TFM-C inhibited secretion of IL-1β, IL-12 and IL-17, enhanced that of TNF-α and RANTES, reduced neuronal axonal damage and protected from oxidative stress in the organotypic model. TFM-C blocked TNF-α release in microglial cells through a process involving intracellular retention, but induced TNF-α secretion in primary astrocyte cultures. Finally, we demonstrate that TFM-C and celecoxib ameliorated EAE with equal potency. This coincided with reduced secretion of IL-17 and IFN-γ by MOG-reactive T-cells and of IL-23 and inflammatory cytokines by bone marrow-derived dendritic cells. Our study reveals that non-coxib analogues of celecoxib may have translational value in the treatment of neuro-inflammatory conditions.

Citation: Di Penta A, Chiba A, Alloza I, Wyssenbach A, Yamamura T, et al. (2013) A Trifluoromethyl Analogue of Celecoxib Exerts Beneficial Effects in Neuroinflammation. PLoS ONE 8(12): e83119. doi:10.1371/journal.pone.0083119

Editor: Giovambattista Pani, Catholic University Medical School, Italy

Received June 14, 2013; **Accepted** October 31, 2013; **Published** December 11, 2013

Funding: This study was supported by Grant Grupos de Investigación (UPV/EHU; ref. IT512-10) to KV; Ministerio de Ciencia e Inovación (MICINN, Madrid, Spain; ref. SAF2008-00433 and SAF2012-32118) and by the Gobierno Vasco's SAIOTEK Program (ref. 'ERtek' S-PE09UN33) to KV; Instituto de Salud Carlos III: FIS PI041445 (MIOTRED) to PV; Juan de la Cierva program of the Ministerio de Ciencia y Innovacion (MICINN, ref. JCI-2009-04462) to AdP. The funders had no role in study design, data collection and analysis, decision to publish, or preparation of the manuscript.

Competing interests: The authors declare that Pablo Villoslada, as one of the co-authors of the manuscript, is a PLOS ONE Editorial Board. This does not alter the authors' adherence to all the PLOS ONE policies on sharing data and materials.

* E-mail: k.vandenbroeck@ikerbasque.org

☯ These authors contributed equally to this work.

Introduction

Nonsteroidal anti-inflammatory drugs are indicated for the treatment of a variety of chronic inflammatory diseases and act by inhibiting prostaglandin H synthase (also known as cyclooxygenase, COX). Two forms of this enzyme are known: COX1 that is expressed constitutively in most tissues and plays a role in the protection of the gastrointestinal mucosa, renal hemodynamics, and platelet thrombogenesis, and COX2 that is inducible and expressed in cells involved in inflammation [1]. Selective COX2 inhibitors (i.e., celecoxib, rofecoxib, and valdecoxib) have been developed for the treatment of inflammatory diseases [2] minimizing gastrointestinal adverse reactions caused by COX-1 inhibition.

Celecoxib has been demonstrated to act via both COX2-dependent and -independent pathways, both associated with potent anti-tumour effects [3,4]. Recently, we have shown that both celecoxib and its trifluoromethyl analogue, TFM-C (4-[5-(4-trifluoromethylphenyl)-3-(trifluoromethyl)- 1*H*-pyrazol-1-yl]benzenesulfonamide) that displays 205-fold lower COX2-inhibitory activity, can inhibit secretion of (hetero)dimeric cytokines belonging to the interleukin-12 (IL-12) family (including IL-23 and p40 homodimers) with similar IC_{50}'s. Using recombinant cell lines, TFM-C caused Ca^{2+}-dependent chaperone-mediated cytokine subunit retention in the endoplasmic reticulum (ER) coupled to degradation via the ER stress protein HERP [5,6]. This observation provided a translational extension of recent findings in our lab of functional chaperone interaction peptide motifs conserved in cytokines as

well as of multiple ATP-dependent cytokine-chaperone interactions during ER transit of cytokines [7-9]. Perturbance of ER Ca^{2+} by celecoxib and non-coxib analogues triggers a cellular response known as "unfolded protein response" (UPR) [4,10,11]. The UPR has a dual role in the cell survival: in normal conditions works as a pro-survival response mediated by the blockage of protein translation and activation of transcription factors that can restore the ER function to its normal physiological state. However, if ER stress persists, its pro-survival function can switch to a pro-apoptotic program, finally leading to cell death [12,13].

COX-2 inhibitors such as indomethacin or rofecoxib exert beneficial effects in EAE; the latter, for example, by modulating Th1/Th2 responses [14,15]. Recently, we have shown that celecoxib inhibits EAE [16]. In particular, we found that celecoxib in contrast to other COX-2 inhibitors such as nimesulid, prevented EAE by inhibiting the infiltration of inflammatory cells into the central nervous system, MOG-specific Th1 cytokine production and expression of adhesion molecules and MCP-1 [16]. This protective effect was not mediated via COX2 inhibition since it was also observed in COX2-deficient mice [16]. We have demonstrated that celecoxib and its analogue TFM-C exerted beneficial effects in two models of arthritis: collagen-induced arthritis (CIA) and collagen antibody-induced arthritis (CAIA). In particular, TFM-C, more so than celecoxib, inhibited the severity of CIA and CAIA by suppressing the activation of mast cells and the production of inflammatory cytokines by macrophages [17]. Nevertheless, celecoxib and other COX2 inhibitors display adverse effects that may compromise further implementation in clinical practice. Increased risk for myocardial infarction and stroke in drug recipients have been reported [18-22]. Comparison of cardiovascular risks profiles of celecoxib vs the non-selective nonsteroidal anti-inflammatory drug naproxen and ibuprofen is currently addressed in the PRECISION trial (http://clinicaltrials.gov/show/NCT00346216). Suppression of prostacyclin (PGI2) and prostaglandin E2, two COX-2-derived products, may provide protective constraint mechanisms on processes such as thrombogenesis and atherogenesis [23]. In rodents, celecoxib predisposes to platelet activation and arterial thrombosis by suppressing PGI2 [24]. Similarly, selective inhibition of COX-2 can enhance platelet–vessel wall interactions and platelet adhesion *in vivo* increasing the risk of thrombosis [25].

We hypothesized that TFM-C may constitute a new drug candidate that retains the beneficial effects of celecoxib in the EAE model while its much decreased COX2 inhibitory activity would render it less adverse in terms of cardiovascular risk. In this study, we have analyzed the effect of TFM-C on cytokine secretion, demyelination, and axonal damage in mice cerebellar organotypic cultures, a model of neuroinflammation, and assessed its activity in the EAE model.

Materials and Methods

Ethics statement

Animals were handled in accordance with the European Communities Council Directive (Directive 2010/63/EU), the Spanish regulations for the procurement and care of experimental animals (RD 53/2013, February 1st), and the study was approved by the Ethical Committee on Animal Research of the University of Basque Country (UPV/EHU). EAE experiments were approved by the Institutional Animal Care and Use Committee of the National Institute of Neuroscience (Tokyo, Japan).

Table 1. List of primary antibodies used for immunofluorescence (IF) and western blot (WB) studies.

Antigen	Description	Dilution	Company
ARMET	ARMET antibody, Rabbit	1:2000 (WB)	AbCam
HERP	Homocysteine-induced endoplasmic reticulum protein, Mouse	1:200/1:400 (IF) 1:2000 (WB)	Hirabayashi Y [6].
Iba1	Ionized calcium binding adaptor molecule 1: anti-Iba 1, Rabbit	1:400/1:500 (IF)	Wako
iNOS	Inducible nitric oxide synthase: purified rabbit anti-iNOS/NOS type II	1:200 (IF) 1:500 (WB)	BD Bioscience
LC3B	LC3B (D11) XP™ Rabbit mAb	1:1000 (WB)	Cell Signaling
MBP	Myelin Basic Protein; Rat anti-MBP (82-87) antibody	1:200 (IF)	Serotec
NFH	Neurofilament heavy (phosphorylated and non-phosphorylated NfH): rabbit polyclonal antiserum against the 200 kD Neurofilament Heavy	1:200 (IF)	AbCam
NFL	Neurofilament light C28E10, Rabbit mAb	1:200 (IF)	Cell Signaling
PARK2	Rabbit polyclonal to Parkin	1:750 (WB)	AbCam
RAB24	Purified Mouse Anti-Rab24	1:1000 (WB)	BD Bioscience
SMI32	non-phosphorylated neurofilament heavy SMI32, Mouse	1:200 (IF)	Stenberg
TNF-α	Anti-Murine TNF-alpha, Rabbit	1:300 (IF)	MBL
Tubulin	α-Tubulin Antibody [HRP], mAb, Mouse	1:2000	GenScript

doi: 10.1371/journal.pone.0083119.t001

Materials and animals

All animal experiments in this study were performed using C57BL/6J mice (Harlan Laboratories, Italy). C57BL/6J Jcl mice used in EAE experiments were purchased from CLEA Japan, Inc. Mice were maintained in a temperature-controlled environment with food and water *ad libitum* at 12-hour light/12-hour dark cycle. The animals used in this study were 8 weeks old for EAE experiments and 8 days old for cerebellar organotypic cultures experiments. TFM-C was synthesized by Onyx Scientific (Sunderland, UK). All antibodies used in this work are indicated in Table 1.

Induction and clinical assessment of EAE

C57BL/6J Jcl (B6) female mice (n = 5-6 per group, 7-8 weeks old) were immunized subcutaneously at the base of the tail with 100 μg of myelin oligodendrocyte glycoprotein 35-55

(MOG35-55) peptide (amino acid sequence, MEVGWYRSPFSRVVHYRNGK, derived from mouse MOG) dissolved in 0.1 ml phosphate buffered saline (PBS) and 0.1 ml CFA containing 1 mg of Mycobacterium tuberculosis strain H37Ra (*Mtb* H37Ra). Shortly after immunization and 48 h later, the mice were injected i.p. with 200 ng of Bordetella pertussis toxin (List Biological Laboratories). Mice were randomly assigned to three treatment groups receiving intraperitoneal injections of TFM-C or celecoxib at doses of 10 µg/g, or control vehicle every other day from the day of immunization. In the control group, the sample size is n=5-6 per group (16 animals in total) and in the TFM-C-treated group n=4-5 animals per group (14 animals in total). The experiment was repeated three times in order to respect the directives for reduction of the number of animals in animal experiments. Only 5 animals were used in the celecoxib-treated group because we have assessed the effect of celecoxib in a previous study [16]. Clinical scores of EAE were assigned daily as follows: 0 = normal; 1 = weakness of the tail and/or paralysis of the distal half of the tail; 2 = loss of tail tonicity; 3 = partial hind limb paralysis; 4 = complete hind limb paralysis; 5= forelimb paralysis or moribund; 6 = death. The EAE scoring was conducted by personnel unaware of treatment-group assignments. Mice were sacrificed with lethal dose of diethyl ether.

Cerebellar organotypic cultures

The cerebellar slice culture was based on published protocols [26,27]. Organotypic slice cultures were prepared from 8-day old C57BL/6 mice. Cerebella were cut at 350 µm with a McIlwain Tissue Chopper (The Mickle Laboratory Engineering Co. LTD.) and three slices were plated on Millicell-CM culture inserts. From 10 mice we obtained approximately 90 slices. Cultures were incubated at 37°C and 5% CO_2 in 50 % basal medium with Earle's salt, 25% Hank's buffered salt solution, 25% inactivated horse serum, 5mg/ml glucose, 0,25mM L-glutamine and 25µg/ml Pen/Strep (Invitrogen). Cerebellar slices were maintained in culture for 7 days and then pre-treated with 50 µM of TFM-C for 2 hours followed by stimulation with 15 µg/ml of lipopolysaccharide (LPS; Sigma L4391) for 6 and 24 hours, or as indicated.

BV2 cell line

BV2 cells were provided by Prof. Carlos Matute (University of the Basque Country, Leioa, Spain) [28] and were maintained in Dulbecco's Modified Eagle's medium (DMEM) containing 5% heat inactivated Fetal Bovine Serum (FBS), 4 mM L-Glutamine (SAFC biosciences), 20 mM Hepes (Sigma) and 25µg/ml Pen/Strep (Invitrogen) antibiotics at 37°C in a humidified chamber with 5% $C0_2$. Before treatment, cells were washed twice with DMEM, then pre-incubated with TFM-C (30 µM or 50 µM) for 2 hours and stimulated with 1 µg/ml LPS (Sigma L4391) for 3, 6, 12 and 24 hours.

HEK-293 cell line and PCR arrays

Human embryonic kidney-293 cells (HEK-293; Invitrogen), were cultured in DMEM (Sigma) supplemented with 10 % fetal bovine serum (Sigma), 2 mM L-glutamine (Invitrogen) and 25µg/ml Pen/Strep (Invitrogen). Cells were washed twice with DMEM and incubated with TFM-C (50 µM) for 3, 6, 12 and 24 hours. RNA was extracted and reverse transcribed using RT^2 First Strand Kits (SABiosciences, address), followed by profiling of the expression of 84 key genes each belonging to UPR, Ubiquitination and Autophagy Pathway RT^2 Profiler PCR Arrays (SABiosciences, address). Data was analyzed using the manufacturer's PCR Array Data Analysis Software.

Total protein extraction and Western Blot

Three cerebellar slices, HEK-293 and BV2 cells were homogenised by stroke dounce homogenization in 60 µl of ice-cold RIPA buffer (150mM NaCl; 50mM Tris-Cl, pH 7.5; 1% NP-40; 0.5% DOC; 0.1% SDS) and the lysate was centrifuged at 15.000 x g for 10 min at 4°C. Total protein concentration was estimated by the Bradford assay (Bio-Rad). 10 µg of total protein from cerebellar slices, BV2 or HEK-293 cells were separated by SDS-PAGE on Bio-Rad TGX Stain-Free precast gels. The gels were exposed to UV irradiation for 5 min and then total protein was transferred onto a nitrocellulose membrane (Bio-Rab). UV irradiation activates a covalent reaction between the trihalocompound and tryptophan residues on the proteins in the gel, resulting in UV induced fluorescence (Figure S5). Total protein was visualized with ChemiDoc (Bio-Rad) and quantified using Image Lab 4.0 software. The filters were pre-wetted in blocking buffer (5% dried non-fat milk or 2% casein, 20 mM Tris pH 8, 300 mM NaCl, 0.1% Tween-20) and then hybridized for 2h or O.N. with primary antibodies in blocking buffer (Table 1); the secondary antibodies (HRP-conjugated anti-mouse or anti-rabbit from Cell Signaling) were used at a dilution of 1:2000.

RNA isolation and Quantitative RT-PCR (QPCR)

Cerebellar organotypic cultures, HEK-293 and BV2 cells were lysed with TRI reagent (Sigma). Chloroform was added for phase separation with RNA remaining in the aqueous phase. RNA was precipitated with 2-propanol and the pellet resuspended in DNA/RNA free water (Invitrogen). RNA was quantified using Nanodrop 2000c spectrophotometer (Thermo Scientific). 200 ng of mice organotypic cultures, HEK-293 and BV2 cells RNA were reverse-transcribed to cDNA using random primers according to manufacturer's protocol (Applied biosystems). QPCR was performed with the Supermix for SsoFast EvaGreen (Biorad) on a 7500 Fast Real-Time PCR System (Applied Biosystems). For each target gene, QPCR QuantiTect Primer Assay were used (Qiagen). Expression levels for the transcripts of interest were normalized to that of endogenous glyceraldehyde 3-phosphate dehydrogenase or hypoxanthine phosphoribosyltransferase 1 (Hprt1). The data were calculated as percentage fold expression or $2^{-\Delta\Delta Ct}$ relative to the average of the untreated control group, unless indicated otherwise.

Quansys Q-Plex™ Array Chemiluminescent and ELISA

For Q-Plex system analysis, 30 µl of medium from mice cerebellar organotypic cultures treated with LPS or LPS/TFM-C were used. Mouse Cytokine Stripwells (16-plex) were used following the manufacturer's instructions (Quansys Bioscience).

The chemiluminescent signal was acquired with Bio-Rad ChemiDoc camera and the image was analyzed with Q-View Software (Quansys Bioscience). BV2 cells were pre-treated with TFM-C (30 μM or 50 μM) for 2 hours and then stimulated with LPS for different periods of time (0, 3, 6, 12 and 24 hours) and the culture supernatants were collected to quantify the secreted IL-1β, tumor necrosis factor (TNF-α) and IL-6. Mouse ELISA Kits were used according to the manufacturer's instructions (eBioscience, BD Bioscience, R&D Systems).

Immunofluorescence microscopy

Cerebellar slices were fixed with 4% paraformaldehyde (PFA) for 40 min, washed with PBS for 10 min, and blocked at RT for 2 hours in 10% normal goat serum (NGS; Vector Laboratories) and 0.5% Triton X-100 in PBS. The slices were incubated overnight at 4°C with the distinct primary antibodies (Table 1) in blocking solution (10% NGS and 0.3% Triton X-100 in PBS). The slices were washed and incubated in blocking solution containing the secondary antibody mixture and washed three times with 0.1% Triton X-100 in PBS. BV2 cells were fixed with 4% PFA for 20 min, washed with PBS for 10 min, permeabilized for 20 min with 0.2% Triton X-100 in PBS and blocked at RT for 30 min in 10% FBS (Invitrogen) in PBS. The cells were incubated 1 hour with the Iba1 and HERP (1:400; kindly supplied by Dr. Yasuhiko Hirabasyashi, Tohuku University, Japan) or TNF-α primary antibodies in blocking solution (10% FBS in PBS). After washing, the cells were incubated in blocking solution containing the secondary antibody mixture, washed three times with PBS and incubated with DAPI (1:50000; Molecular Probes) in PBS. The secondary antibodies used were mouse IgG Cy2-linked, rabbit IgG Cy3-linked (from goat, 1:200; GE Healthcare) and goat anti-rat IgG Alexa Fluor 488 (1:200; Molecular Probes). The slices and coverslips were mounted in Gel/Mount anti-fading mounting medium (Biomeda) and pictures were captured by confocal scanning microscopy (Olympus Fluoview FV500) from single images all through the whole tissue or cells (but avoiding the surface of the culture in contact with air).

DAPI and Propidium iodite (PI) staining

12 hours before LPS/TFM-C (3, 6, 12 and 24 hours) treatment BV2 cells were incubated over night with PI (250 ng/ml; Fluka) and then fixed with 4% PFA. The cells were washed three times with PBS and then incubated with DAPI (1:50000; Molecular Probes) in PBS. Coverslips were embedded in Fuoro-Gel (Electron Microscopy Science). Images were recorded using the confocal microscope and analyzed using the ImageJ program (version 1.40).

Flow cytometry of BV2 cells

The expression of intracellular TNF-α was evaluated by cytofluorometry. $1x10^6$ cells were plated and after 24 hours treated with LPS (1μg/ml) or pre-treated with TFM-C for 2 hour and then stimulated with LPS/TFM-C for 3, 6, and 24 hours. The cells were detached with trypsin, washed in PBS, pelleted at 300 g for 10 min and fixed with PFA 2% for 20 min. Then, cells were permeabilized with 0,2% Triton in PBS for 20 min, blocked with 10% NGS in PBS for half hour, and incubated with primary antibody TNF-α (1:100; MBL) for 1 hour in blocking solution. After washing, cells were incubated with secondary antibody (1:500 goat anti-mouse AlexaFluo 488; LifeTechnology) in blocking solution for 30 min in darkness. Following further washes, cells were pelleted and the fluorescence was analyzed using a Gallios cytometer (Beckman Coulter) at excitation/emission wavelengths of 488/515-535 nm.

Astrocyte-enriched cell culture

Primary cultures of cerebral cortical astrocytes were prepared as described previously by McCarthy and de Vellis (1980) [29]. Briefly, forebrains were removed from the skulls, the meninges were carefully excised under a dissecting microscope, and the cortices were isolated. Tissue was incubated for 15 min in Hank's Balanced Salt Solution (HBSS) with tripsine and DNAase, the reaction was stopped with DMEM supplemented with 10% FBS and centrifuged to remove cellular debris. Cells were resuspended in Iscove's Modified Dulbecco's Medium supplemented with 10% FBS and antibiotic/antimycotic solution, and the cells were dissociated by passage through needles of decreasing diameter (21 G and 23 G) 10 times. Cells were re-centrifuged and then resuspended in Iscove's Modified Dulbecco's Medium supplemented with 10% FBS and antibiotic/antimycotic solution. Cells were seeded into poly-D-lysine-coated flasks, and maintained in culture at 37°C and 5% CO_2. The culture medium was renewed the day after seeding, and twice a week thereafter. After 8 days, cultures were shaken (3 hours, 350 rpm) to deplete microglial cells and were trypsinized and plated onto poly-D-lysine-coated, 24-well plates.

Statistical analysis

All experiments were performed at least three times, and control cultures were time-matched with testing cultures. The values were expressed as the means ± SEM. ANOVA or Student's t-tests were used to determine statistical significance, as indicated, and all analyses were performed using SPSS 15.0 software (IBM). EAE clinical or pathological scores for the group of mice are presented as the mean group clinical score +SEM, and statistical differences were analyzed with a non-parametric Mann-Whitney U-test.

Results

TFM-C modulates cytokine release and suppresses oxidative stress and axonal damage in mouse celerebellar organotypic cultures

The effect of TFM-C on cytokine release was assessed in a model of neuroinflammation consisting of mice cerebellar organotypic cultures stimulated with LPS, by means of a multiplex ELISA-based Q-Plex assay system (see Materials and Methods). Of 16 assessed cytokines, 5 were identified of which LPS-induced secretion was modulated by TFM-C (Figure 1A). While LPS challenge induced varying levels of the pro-inflammatory cytokines IL-1α, IL-1β, IL-3, IL-5, IL-6, IL-10, IL-12, IL-17, MCP-1, IFN-γ, TNF-α, MIP-1α and RANTES

(Figure 1A), TFM-C treatment significantly decreased IL-1β, IL-12 and IL-17 release and increased TNF-α and RANTES. mRNA levels of a subset of these cytokines were also measured in mice organotypic cultures treated with LPS or LPS/TFM-C. HERP was included as a marker for ER stress that is inducible by TFM-C [6,9]. TFM-C treatment decreased IL-1β mRNA expression levels at 6 and 24 hours, but those of IL-6 and IL-10 only at 24 hours (Figure 1B). In contrast, TNF-α mRNA levels were significantly higher after 6 hours of TFM-C treatment and this trend persisted at the 24 h time-point (non-significant). This mirrored the increased levels of secreted TNF-α demonstrated in Figure 1A. No significant changes were observed for IL-12p35, IL-23p19 and HERP mRNAs.

Next we scored the effect of TFM-C on LPS-induced oxidative stress, demyelination and axonal damage in the organotypic model [30-33] using immunofluorescence, immunoblot and QPCR. The analyzed markers included iNOS for oxidative stress, CNPase for demyelination, SMI32 for axonal damage, and HERP for ER stress. Immunofluorescence showed that TFM-C increased HERP protein expression in microglia identified with Iba1, and upregulated HERP protein in the total culture (Figure 2A, panel a; Figure 2B). Axonal damage was visualized by dual immunostaining for both total (phosphorylated and non-phosphorylated) NFH and non-phosphorylated NFH (SMI32; Figure 2A, panel d). In response to LPS, non-phosphorylated NFH was found to accumulate at 3.5 higher levels compared to total NFH, suggestive for induction of axonal dysfunction. Furthermore, LPS-induced axonal damage was visible via formation of swollen structures (beading and spheroids; white box in Figure 2A, panel d) associated with impaired axonal transport and transection [34]. TFM-C prevented formation of swollen structures and maintained LPS-induced non-phosphorylated neurofilament levels to those of baseline control (Figure 2D). In contrast, TFM-C treatment had no effect on demyelination assessed by MBP/NFL immunofluorescence (Figure 2A, panel c) or CNPase expression (Figure 2B). Finally, pretreatment with TFM-C prior to LPS challenge strongly reduced iNOS expression determined by immunofluorescence, Western Blot and QPCR (Figure 2A, panel b; Figure 2B & C). TFM-C did not affect expression of MHCII (Figure S1). Taken together, these results indicate that TFM-C partially counteracted LPS-induced effects reminiscent of an anti-inflammatory, anti-oxidant and neuroprotective mode of action.

TFM-C suppresses cytokine release and induces UPR / ER stress in BV2 microglia cells

Previously, we have demonstrated that TFM-C inhibits secretion of the (hetero)dimeric IL-12 family cytokines IL-12, $p40_2$ and IL-23 through a Ca^{2+}-dependent mechanism involving chaperone-mediated cytokine retention in the ER coupled to degradation via HERP protein, and that TFM-C dramatically upregulates *HERP* gene expression in various cell lines [5,6,9]. In organotypic cultures, virtually no effect was seen on mRNA production of *HERP* at 6 and 12 hours of LPS/TFM-C treatment in compared with LPS stimulation (Figure 1B). To verify whether TFM-C is capable of inducing ER stress in microglia, the mouse microglial BV2 cell line was used. Specifically, we measured mRNA of HERP and IL-23p19, both of which are induced by ER stress [5,6,35]. BV2 cells were pre-treated with TFM-C (30 and 50 μM) for 2 hours and then stimulated with LPS for 3, 6, 12 and 24 hours in the presence or absence of TFM-C, which showed significant dose-dependent up-regulation of IL-23p19 and HERP (Figure 3B). Figure 3C shows that co-treatment of LPS with TFM-C led to increased accumulation of HERP in microglial cells (Figure 3C, panel a). In immunoblot, HERP protein levels were increased in BV2 cells at 12 hours of treatment in the presence of 50 μM of TFM-C plus LPS compared to LPS-only challenge (Figure 3C, panels b and c; Figure S5). To answer the question whether TFM-C is also able to block cytokine release from BV2 cells, IL-1β, IL-6 and TNF-α mRNA and secreted protein levels were analyzed (Figure 3A). TFM-C significantly decreased LPS-induced IL-1β mRNA and protein secretion starting at 6 hours of treatment. However, TFM-C exerted biphasic opposing effects on TNF-α mRNA levels at 3 (decrease) versus 24 (increase) hours compared to LPS-only challenge; of note, TFM-C suppressed secreted TNF-α protein levels throughout the duration of the experiment. For IL-6, no significant changes were observed in mRNA levels while the secreted protein was down-regulated at 12 hours of TFM-C treatment. To rule out occurrence of apoptotic cell death as contributing factor in suppression of cytokine secretion, cells were stained with DAPI and PI which is only incorporated by cells that have suffered membrane damage. TFM-C/LPS treatment decreased cell viability with approximately 4%, similar to LPS-only treated cells (Figure 3D). To identify additional UPR/ER stress-regulated genes potentially involved in altered cytokine folding/assembly/secretion, the effect of TFM-C on transcription of 252 genes belonging to UPR, autophagy and ubiquitination pathways was analyzed in HEK-293 cells (Figure S2A). We identified 36 genes with a fold increase > 2.5 and confirmed *HERP* as the gene showing the fifth highest degree of upregulation by TFM-C (fold increase of 9.1 in the UPR PCR Arrays). *DDIT3* (CHOP), a primordial ER stress response gene [13,36], was identified with some distance as the gene showing the highest degree of induction by TFM-C (36-fold). Further analysis of the kinetics of upregulation by TFM-C of 5 of these genes, *PARK2, ARMET, FBXO4, RAB24* and *MAP1LC3B*, in addition to *HERP*, was performed in both HEK-293 and BV2 cells (Figure S2B and S2C). At the protein level, only HERP, MAP1LC3B and ARMET showed clear changes in the kinetics of their production in HEK-293 cells. In BV2 cells, TFM-C significantly decreased PARK2 expression at 3 and 12 hours, and increased RAB24 expression at 3 hours both compared with LPS-treated cells. No modification in MAP1LC3B and ARMET protein expression was observed (Figure S2D). Thus, TFM-C induces a gene expression signature predominantly enriched for UPR/ER stress response and ubiquitination pathway genes, including to a lesser extent also some genes involved in autophagy (Figure S2A). Pending mechanistic studies, this suggests that its suppressive effect on cytokine secretion may be functionally related to alterations in protein transit and turnover pathways, as suggested in our previous work [5,6,9,17].

A a

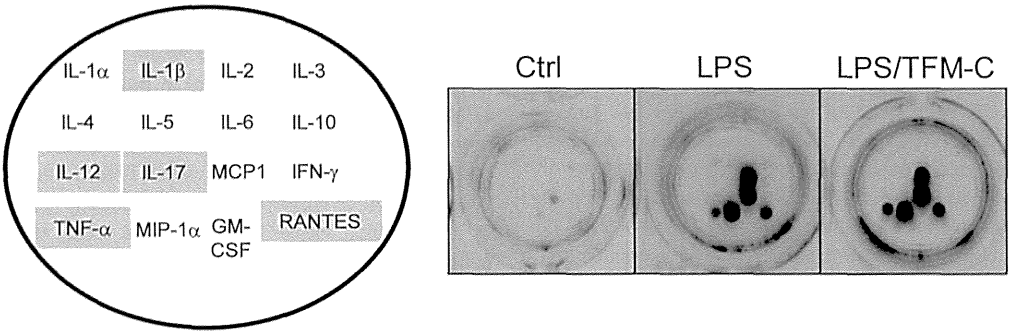

b

Cytokine	Ctrl pg/ml ±sd	LPS pg/ml (±sd)	LPS/TFM-C pg/ml (±sd)	% increase or decrease
IL-1α	9,7±5,4	31,8 (±13,5)	34,6)±17,2)	+8,1
IL-1β	70,7±37,4	299,9 (±26,2)	234,3 (±20,4)*	-21,9
IL-2	ND	ND	ND	ND
IL-3	ND	31,5 (±6,4)	16,2 (±11,8)	-48,6
IL-4	8,3±10,4	18,1 (±3,7)	10,5 (±7,6)	-42,3
IL-5	2,0±4,9	331,2 (±56,4)	431,4 (±58,7)	+30,2
IL-6	ND	4125,2 (±270,8)	4144,0 (±140,2)	+0,5
IL-10	ND	25,9 (±1,9)	25,1 (±3,7)	-3,1
IL-12p70	5,6±5,9	73,4 (±21,8)	33,6 (±8,9)*	-54,6
IL-17	ND	102,5 (±26,9)	54,7 (±9,9)*	-46,6
MCP-1	ND	2237,3 (±124,0)	2240,9 (±104,8)	+0,3
IFN-γ	12,3±19,5	91,8 (±20,5)	70,0 (±20,0)	-23,8
TNF-α	2,0±2,4	229,4 (±35,2)	436,6 (±27,1)*	+90,3
MIP-1α	ND	6354,5 (±351,2)	6243,2 (±283,9)	-1,7
GMCSF	ND	ND	ND	ND
RANTES	6,3±4,6	3649,3 (±182,2)	11340,0 (±2800,1)*	+210,7

B

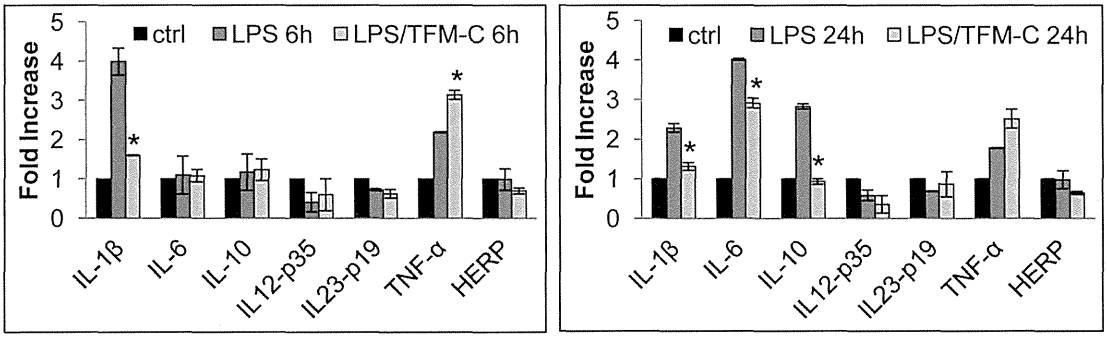

Figure 1. Effect of TFM-C on cytokine production in organotypic cerebellar cultures. A) After 7 *DIV* organotypic cultures were treated with TFM-C (50μM) for 6h and then stimulated with 15μg/ml LPS for 24h in presence of TFM-C. Panel a) Lay-out of cytokine-specific antibody spots in the 16-plex cytokine Stripwell array (left image) and visualization of cytokine-specific chemiluminescence in culture medium of LPS-treated organotypic cultures in the absence or presence of TFM-C (right images). Cyotkine levels significantly affected by TFM-C are highlighted in grey. Panel b) pg/ml of cytokines were indicated. sd: standard deviation. ND: not determinable. B) Effect of TFM-C on IL-1β, IL-6, IL-10, IL-12p35, IL-23p19, TNF-α and HERP mRNA in organotypic cultures stimulated by LPS for 6h and 24h in presence or absence of 50μM TFM-C. The levels of mRNA are shown as *n*-fold increase compared with baseline level (-) and normalized to those of the housekeeping gene *Hprt1*. Asterisks indicate significant differences at *<*P* 0.05 compared with LPS control by ANOVA test.

doi: 10.1371/journal.pone.0083119.g001

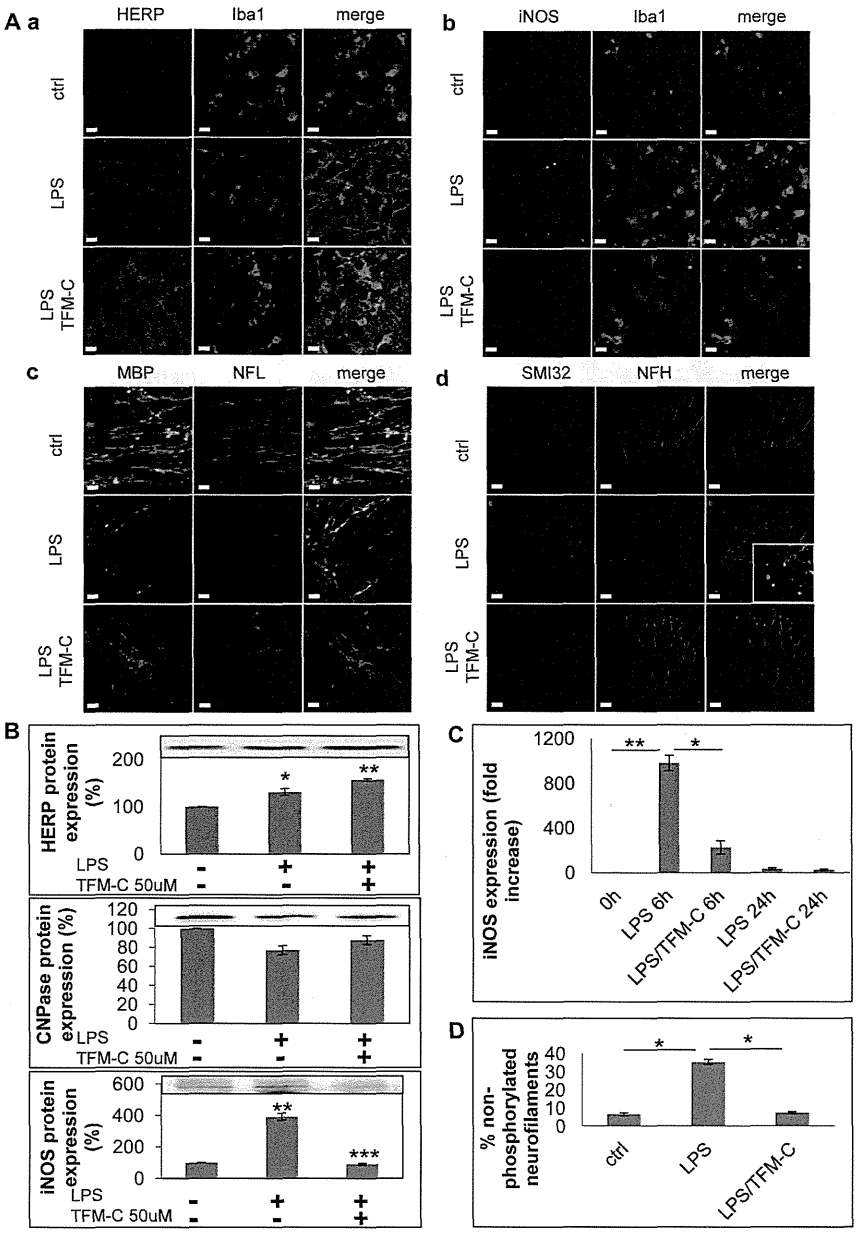

Figure 2. Effect of TFM-C on ER stress, oxidative stress, demyelination and axonal damage in organotypic cerebellar cultures. A) Organotypic cultures were stimulated with LPS for 24h or pre-treated with TFM-C (50μM) for 2h and then stimulated with LPS/TFM-C for 24h. Panel a-b: immunostaining for Iba1 (red) and HERP or iNOS (green). Panel c: immunostaining for NFL (red) and MBP (green); Panel d: immunistaining for total neurofilament-heavy (NFH; red) and non-phosphorylated neurofilament (SMI32; green). In the white box inset are shown axonal spheroids and occurrence of axonal transection (end-bulbs). Scale bar 10μm. B) 10μg of total protein were loaded for HERP, CNPase and iNOS Western blot analysis. Quantification of band intensity was calculated in the graphs below after normalization for total protein loaded. Results are expressed as percentage compared to the LPS only (100%). Error bars indicate the standard error. **P*<0.05, ***P*<0.001, ****P*<0.001 by ANOVA test. C) After 7 *DIV* organotypic cultures were treated with TFM-C for 2h and then stimulated with 15μg/ml LPS for 6 and 24h. iNOS mRNA expression was analyzed by quantitative PCR. The levels of mRNA are shown as *n*-fold increase compared with the level of baseline condition (-) and normalized to those of the housekeeping gene *Hprt1*. All values represent the averages of three independent experiments. Error bars indicate the standard error. **P*<0.05, ***P*<0.01, ****P*<0.001 by ANOVA test. D) Percentage of non-phosphorylated neurofilaments with respect to total neurofilaments in cerebellar cultures stimulated for 24h with LPS in presence or absence of TFM-C. Error bars indicate the standard error. **P* <0.05 by ANOVA test.

doi: 10.1371/journal.pone.0083119.g002

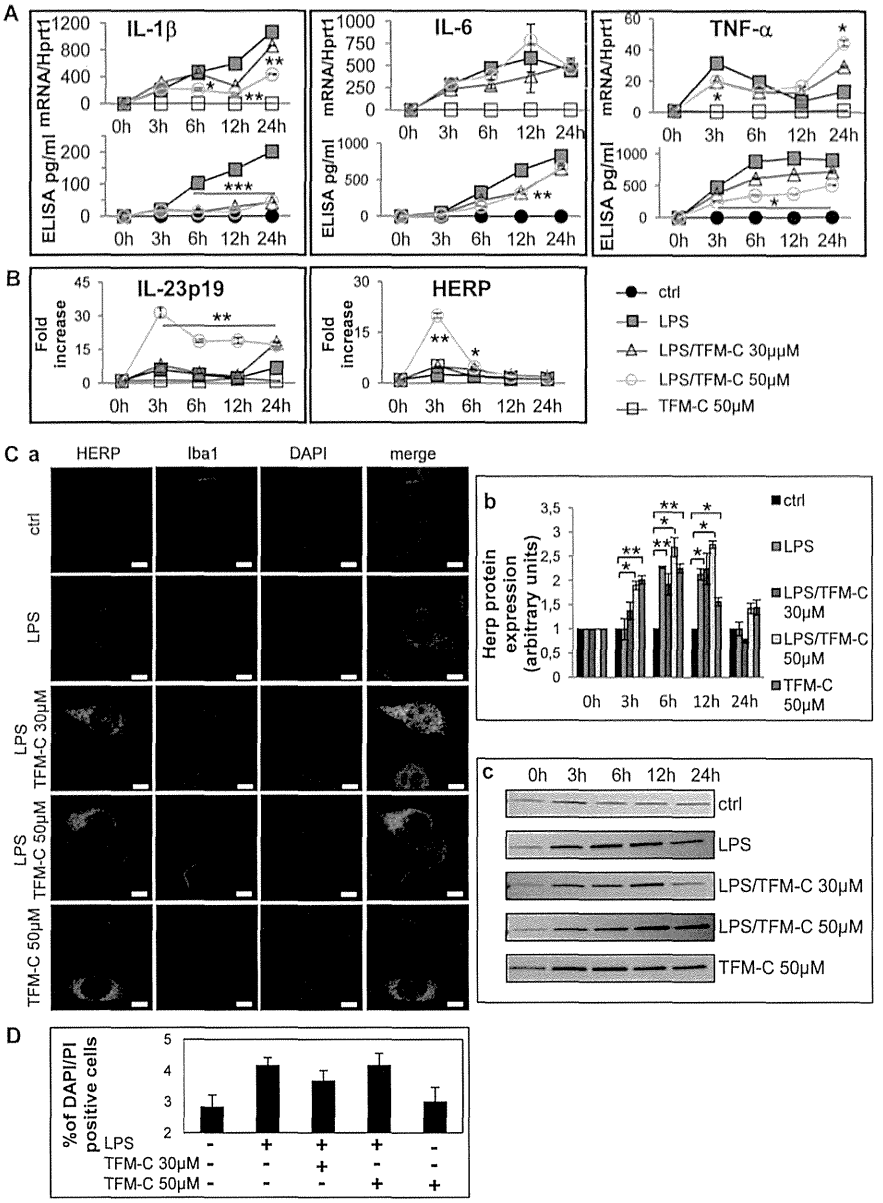

Figure 3. Effect of TFM-C on HERP and cytokine mRNA and protein production in BV-2 cells. BV2 cells were treated with TFM-C (30 or 50μM) for 2h and then stimulated with LPS (1μg/ml) for different times in presence or absence of TFM-C. A) Quantification of the kinetics of mRNA production and cytokine secretion (IL-1β, IL-6 and TNF-α). All values represent the averages of three independent experiments. Lower graphs represent cytokine-specific mRNA quantified by QPCR, while the upper graphs represents amount of secreted cytokine quantified using specific ELISA kits. Asterisks indicate significant differences at $*P< 0.05$, $**P<0.01$, $***P<0.001$ between TFM-C-treated and LPS-treated cells at each time point using ANOVA test. B) Effect of TFM-C (30 and 50μM) on IL-23p19 and HERP mRNAs in BV2 cells stimulated with LPS. The levels of mRNA levels are shown as fold increase. Asterisks indicate significant differences at $*P < 0.05$ and $**P<0.01$ compared with LPS only using ANOVA test. C) Effect of TFM-C on HERP protein expression. BV2 cells were treated with TFM-C (50μM) or pretreated with TFM-C for 2h (30 and 50μM) and then stimulated with LPS in presence of TFM-C. Panel a) Immunofluorescence for HERP (green), Iba1 (red) and DAPI (blue) at 12h of LPS/TFM-C or TFM-C treatment. Scale bar 5μm. Panel b-c) 10μg of total protein were loaded for HERP Western blot analysis. Results were expressed as arbitrary units respect to the control at same time point. Error bars indicate the standard error. $*P<0.05$ by ANOVA test. D) Effect of TFM-C treatment (50μM) on the viability of BV2 cells. Apoptotic cells were measured by double propidium iodite (PI) and DAPI staining, and the percentage of damaged DNA and condensed chromatin was calculated at 24h of LPS/TFM-C treatment.

doi: 10.1371/journal.pone.0083119.g003

TFM-C induces intracellular retention of TNF-α in BV2 microglia but increases its secretion from primary astrocytes

As demonstrated in Figure 3A, TFM-C reduces secreted levels of IL-1β and TNF-α from BV2 microglial cells. To clarify whether TNF-α was retained intracellularly, an immunofluorescence approach was used to monitor subcellular distribution of TNF-α in the ER/Golgi compartment (in permeabilized cells) or at the plasma membrane (in nonpermeabilized cells). BV2 cells treated with LPS exhibited pronounced intracellular TNF-α staining at 3, 6 and 24 h (Figure 4A, panel a). Co-treatment with TFM-C further enhanced intracellular staining of TNF-α, which was validated by flow cytometry and densitometric analysis (Figure 4A panels a and b, and Figure S3). No significant differences were observed in TNF-α staining at the plasma membrane in nonpermeabilized cells between TFM-C/LPS- and LPS-treated cells (Figure S4). This data suggests that the enhanced levels of secreted TNF-α in TFM-C/LPS-treated organotypic cerebellar cultures (Figure 1A) is unlikely to originate from microglial cell sources. Therefore, we analyzed TNF-α production from isolated primary cortical astrocytes, another LPS-inducible natural source of TNF-α in the Central Nervous System (CNS) [37]. As shown in Figure 4B, astrocyte cultures treated with TFM-C alone displayed marginally increased TNF-α release compared with untreated cultures. However, treatment with LPS/TFM-C induced a 2-fold increase in TNF-α secretion compared with the cultures stimulated with LPS only. This result demonstrates that resident astrocytes in the cerebellar organotypic cultures rather than microglia may constitute the source of TNF-α by TFM-C (Figure 1A).

TFM-C suppresses EAE

Previously we demonstrated that celecoxib inhibited EAE in COX-2-deficient mice [16], associated with reduced MOG-specific Th1 cytokines. Thus, TFM-C treatment might be inferred to exert an effect on autoreactive T cells by suppressing production of these cytokines. We examined the effect of TFM-C on EAE induced by immunization with MOG derived peptide, MOG35-55, in which disease development largely depends on encephalitogenic T cells. The administration of TFM-C reduced the severity of EAE when compared with the control group (Figure 5). The incidence of disease in the control group was 93.8% and TFM-C reduced the incidence to 57.1%. The average day of onset was 15.2±3.1 in control group and 16.4 ±2.5 in the TFM-C-treated group. This result indicates that TFM-C limits the severity of disease showing similar effects to celecoxib [16].

TFM-C suppresses IFN-γ and IL-17 production from MOG-reactive T cells

We next examined the effect of TFM-C on MOG35-55-specific T cell responses by *ex vivo* re-challenge with MOG35-55 peptide 10 days after immunization. The proliferative response to MOG35-55 was slightly reduced in celecoxib-treated mice (Figure 6A). TFM-C exhibited a stronger inhibitory effect on MOG35-55-reactive T cell proliferation, even though the overall effect of TFM-C on proliferation was also

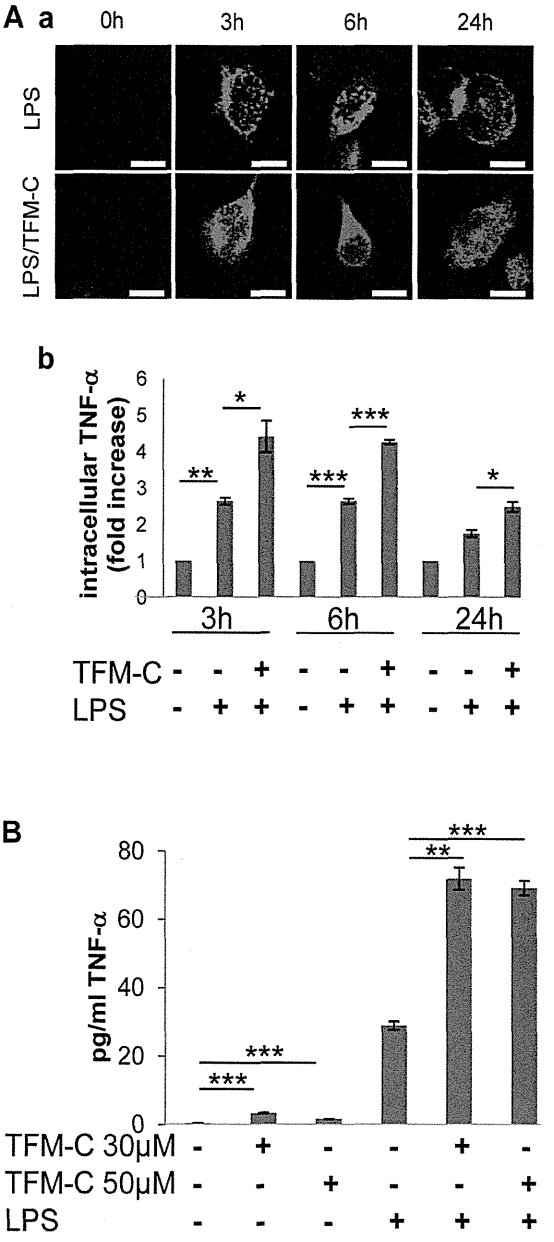

Figure 4. Intracellular localization of TNF-α in BV2 cell line and TNF-α secretion in primary astrocytes. A) BV2 cells were treated with TFM-C (50μM) for 2h and stimulated with LPS (1μg/ml) for 3, 6 and 24h in presence or absence of TFM-C. Panel a) Staining for TNF-α in permeabilized cells. Scale bar 5μm. Panel b) Intracellular localization of TNF-α by flow cytometry. Results are expressed as fold increase compared to the control at the same time point. B) TNF-α release in astrocyte cultures. Astrocytes were treated with TMF-C (30 or 50μM) for 24h or pre-treated with TMF-C for 2h and then stimulated with LPS (1μg/ml) in presence or absence of TFM-C for 24h and then analyzed by ELISA. Error bars indicate the standard deviation. **P*<0.05, ***P*<0.01, ****P*<0.001 by ANOVA test.

doi: 10.1371/journal.pone.0083119.g004

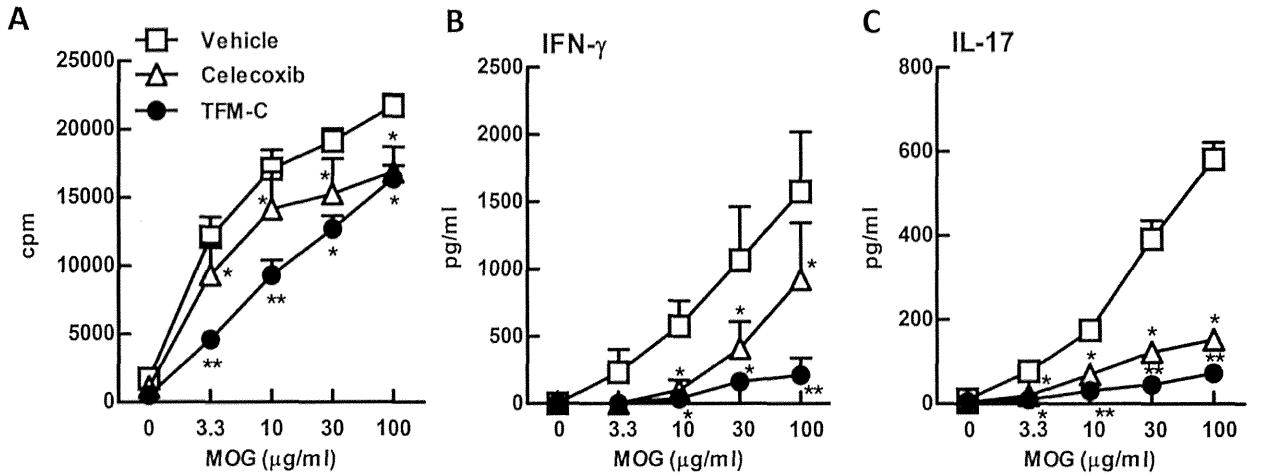

Figure 6. MOG35-55 specific T-cell responses in mice treated with TFM-C. A) Popliteal and inguinal lymph node cells from TFM-C-, celecoxib-treated or control mice were incubated in the presence of MOG35-55 for 48h. Proliferative responses were determined by the uptake of [^{3}H] thymidine. B and C). The levels of IFN-γ and IL-17 in culture supernatants were measured by ELISA. The data shown are from a single experiment representative of three similar experiments. Error bars represent + SEM of 3 mice per group. *P<0.05 compared with control group, **P<0.05 compared with both control and celecoxib-treated groups.

doi: 10.1371/journal.pone.0083119.g006

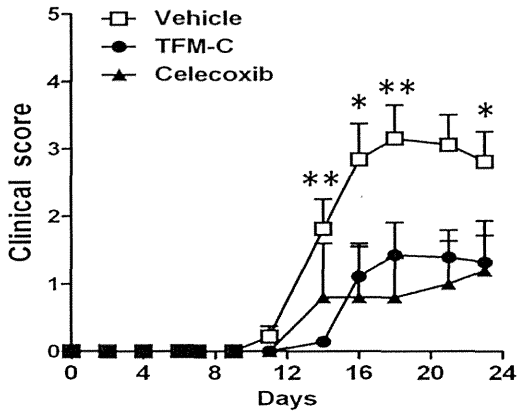

Figure 5. The effect of TFM-C on EAE. Clinical EAE scores of female B6 mice following immunization with MOG35-55. The mice were injected i.p. with 10 μg/kg TFM-C (closed circles), celecoxib (closed triangles) or vehicle (open squares) every other day starting on the day of immunization. *P<0.05 TFM-C-treated versus vehicle-treated group. Results shown are the mean + SEM of 14-16 mice per group in TFM-C- or vehicle-treated groups and of 5 mice in the celecoxib-treated group. The data shown are pooled data from three similar experiments.

doi: 10.1371/journal.pone.0083119.g005

limited (Figure 6A). Compared to control cells, lymph node cells from MOG35-55-primed TFM-C-treated mice produced significantly lower levels of IFN-γ; this was also true for lymph node cells from celecoxib-treated mice albeit to lesser degree (Figure 6B). Furthermore, the level of IL-17 was also significantly reduced in both TFM-C and celecoxib-treated mice compared to that in control mice (Figure 6C). The level of IL-4 was below detection limits (

< 5 pg/ml) (data not shown). These results indicate that TFM-C suppresses MOG35-55-specific T cell proliferation and the production of IL-17 and IFN-γ, and that the suppressive effects of TFM-C on MOG35-55-specific T cell responses are stronger than those of celecoxib.

TFM-C inhibits the production of IL-23 and inflammatory cytokines by dendritic cells

To assess the effect of TFM-C on natural production of IL-12/IL-23, we stimulated Bone Marrow-derived Dendritic Cells (BMDCs) with LPS with or without TFM-C or celecoxib, and measured IL-12 and IL-23 in the culture supernatants. As shown in Figure 7A, IL-23 production was significantly suppressed in the presence of TFM-C. IL-23 suppression was also observed for BMDCs in the presence of celecoxib although the difference did not reach statistical significance. In contrast, neither compound inhibited IL-12 production. To examine the effect on the production of inflammatory cytokines, we stimulated BMDCs with heat-killed *Mtb*, a potent IL-1 stimulator, with or without TFM-C or celecoxib. As shown in Figure 7B, IL-1β, IL-6 and TNF-α production were inhibited in the presence of TFM-C or celecoxib. These results indicate that TFM-C inhibits the production of IL-23 and inflammatory cytokines by BMDCs.

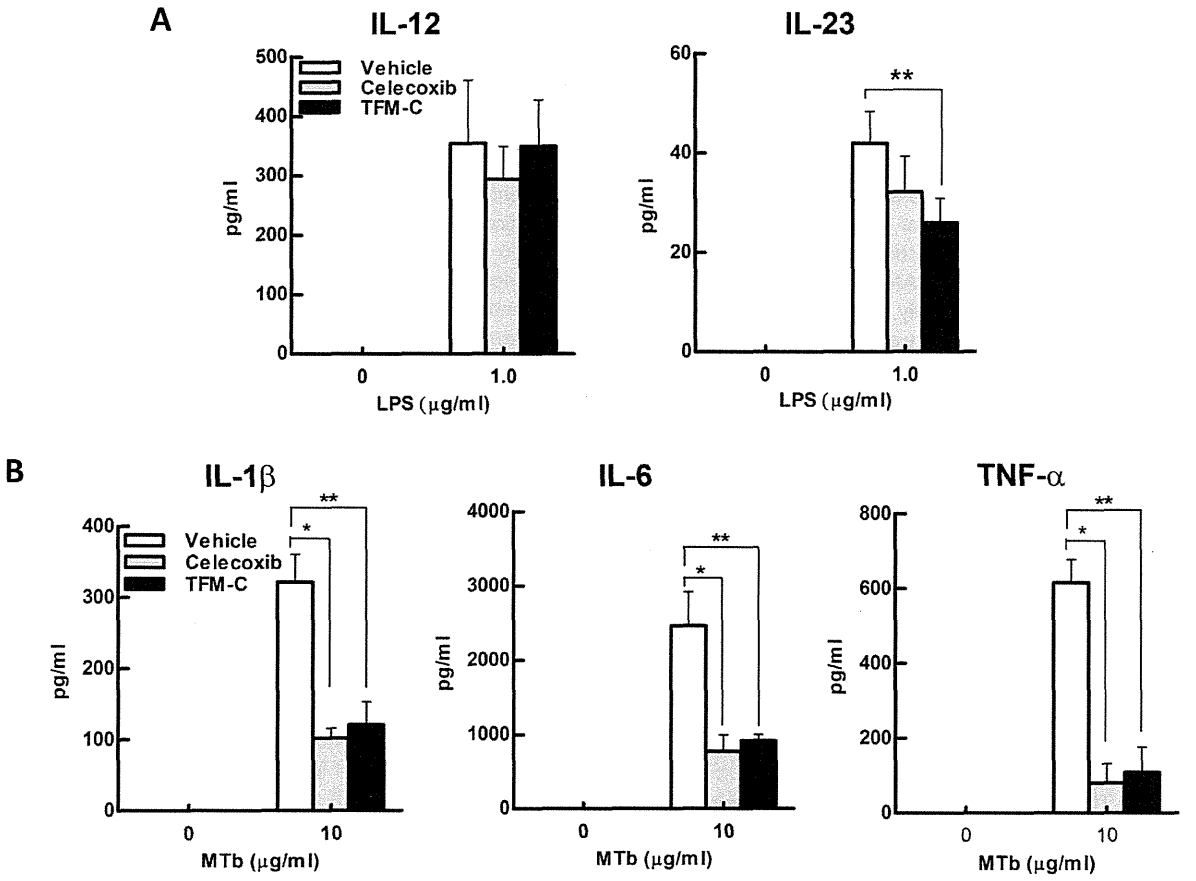

Figure 7. The effect of TFM-C on cytokine production from BMDCs. BMDCs were incubated in TFM-C, celecoxib or vehicle for 16h and subsequently stimulated with LPS (0.1μg/ml) (A) or heat killed H37Ra Mtb (10μg/ml) (B) in the presence of TFM-C, celecoxib or vehicle. Cytokines were detected by ELISA. IL-12, IL-1β or IL-6 were measured 24h after stimulation. IL-23 and TNF-α were measured 6h after stimulation. The data shown are pooled from two similar experiments. Error bars represent + SEM. **P*<0.05 control versus TFM-C celecoxib-treated group, ***P*<0.05 control versus TFM-C -treated group.

doi: 10.1371/journal.pone.0083119.g007

Discussion

In this study, we have tested a non-coxib analogue of celecoxib, TFM-C, both in a model of neuroinflammation consisting of organotypic cultures challenged with LPS [32] and in EAE. The former model recapitulates several events that occur during brain inflammation, including microglia activation followed by cytokine release and oxidative stress, demyelination and axonal damage and permits to study the effect and the mechanism of new treatments for neuroinflammatory disorders [31,32]. Of note, TFM-C significantly decreased axonal damage and oxidative stress in organotypic cultures associated with suppression of IL-1β, IL-12 and IL-17 secretion but enhanced that of TNF-α and RANTES. Similarly to celecoxib in EAE, TFM-C reduced infiltration in CNS, demyelination and production of IFN-γ and IL-17. Further analysis showed that astrocytes cultures treated with TFM-C increased TNF-α release. Moreover, we observed a 2-fold increase in the TNF-α secretion when the astrocytes were co-treated with LPS/TFM-C for 24 hours compared with the cultures stimulated with LPS only. In contrast, in the BV2 microglia cell line, TFM-C suppressed secreted TNF-α protein levels. An explanation for these opposite effects should be sought in the differential response of astrocytes and microglia to modulation of intracellular calcium homoeostasis through selectively inhibiting ER Ca^{2+}-ATPases by celecoxib or TFM-C [5,38]. Astrocytes possess an intracellular Ca^{2+}-dependent excitability leading to glutamate release [39-44]. For example, A23187, a Ca^{2+}-dependent ER stressor, induces elevation of calcium levels, thus increasing glutamate release [45]. In addition, stimulation of astrocytes by glutamate or ATP induces a glutamatergic response accompanied by TNF-α release [46]. However, ionomycin, another Ca^{2+}-dependent ER stressor, does not induce cytokine release in microglia, indicating that in microglia Ca^{2+} perturbation is not sufficient to induce cytokines secretion [47]. These data suggest that the resident astrocytes

and microglia in our cerebellar organotypic cultures respond differentially to Ca^{2+} perturbation by TFM-C in terms of TNF-α secretion.

We also observed a significant increase of RANTES levels in organotypic cultures treated with TFM-C. RANTES is a chemokine that promotes the recruitment and activation of inflammatory cells such as monocytes, lymphocytes, mast cells and eosinophils [48-51]. RANTES also attracts memory T cells, promoting the formation of mononuclear infiltrates characteristic of MS [49,52]. Moreover, it has been described that astrocytes can generate RANTES after stimulation with TNF-α, IL-1β and IFN-γ. Actually, RANTES can be induced only by TNF-α alone in rat primary astrocytes [53].

The role of TNF-α in the pathogenesis of inflammatory demyelinating disease of the central nervous system has been demonstrated in rodents [54] and in humans [55-57]. Transgenic mice that constitutively express TNF-α in the CNS can trigger the development of a chronic inflammatory demyelinating disease [58]. TNF-α is synthesized as a transmembrane precursor protein (tmTNF) and its cytoplasmic tail is cleaved by the TNF-α-converting enzyme (TACE) to release a soluble TNF-α (sTNF). These two forms of TNF-α interact with the receptors, tumor necrosis factor 1 (TNFR1) and 2 (TNFR2). TNFR1 is expressed in all cell types and is preferentially bound by sTNF whereas TNFR2 is expressed by endothelial cells and immune cells and especially bound by tmTNF [59]. The activation of TNFR1 can induce either activation of NFκB or apoptosis via caspase 8 and 3 [60]. The binding to TNFR2 induces proinflammatory and survival signaling pathways [61]. Comparison of TNFR1 and TNFR1/TNFR2 knockout and wild-type mice, shows that EAE symptoms were milder or absent in the knockout animals. In contrast, in TNFR2-deficient mice the symptoms were enhanced and associated with high inflammation and demyelination [62,63]. Remyelinated function was conferred to TNFR2 whereas demyelination to TNFR1 [64]. Recently, we have shown that demyelination was significantly attenuated in cerebellar cultures challenged with LPS pretreated with Fc-TNFR1 recombinant protein [32]. In particular, we found that myelin damage and oligodendrocyte loss were promoted by pro-inflammatory cytokines such as TNF-α. Probably, the observation that the TFM-C treatment had no effect on demyelination in organotypic culture model could be explained by increased astrocytic TNF-α, that in turn induces TNFR1 activation. Moreover, immune cells expressing TNFR2 are lacking in organotypic cultures. In contrast, in the same model TFM-C exerts beneficial effects restoring oxidative stress and axonal damage induced by LPS.

In the EAE model, although the treatment with TFM-C failed to completely inhibit the development of EAE, TFM-C significantly reduced the severity of the disease decreasing the incidence from 93.8% to 57.1%. Moreover, TFM-C suppressed the production of IL-23 and inflammatory cytokines, IL-1β, IL-6 and TNF-α from dendritic cells and this suppressive effect was strong enough to decrease the subsequent production of IL-17 and IFN-γ from lymph node cells upon stimulation with MOG. The differential effects observed on IL-23 inhibition by celecoxib vs TFM-C suggest a beneficial effect of the latter via inhibition of the Th17 responses. In addition to the suppression of IL-23, blockage of IL-6 and IL-1β, two cytokines that affect development of Th17 cells, would also contribute to the suppression of IL-17 [65,66]. TNF-α, IL-1β and IL-6 can increase the permeability of the blood-brain barrier (BBB) [67]. IL-6 induces leukocyte chemoattraction to the endothelium, as well as lymphocyte activation. IL-6 is found in high concentrations in active MS lesions [68,69]. In EAE, IL-6 induction is found in the spinal cord [70]. The detrimental role of IL-6 in this model, associated with BBB permeability, is evidenced in IL-6-deficient mice that are resistant to the pathophysiological alterations [71]; on the other hand, mice overexpressing astrocytic IL-6 showed indeed breakdown of the BBB [72]. Moreover, the inhibition of IL-6 in BMDCs and macrophages [17] treated with TFM-C might suggest that the beneficial effect of TFM-C in EAE can depend on its ability to reduce BBB permeability.

The different effect of TFM-C observed in CNS-derived cells versus lymph node-derived cells may reside in incomplete penetration of TFM-C into CNS. In the *in vivo* system, TFM-C may exert a beneficial effect on peripheral cells, reducing proliferation and pro-inflammatory cytokine secretion, thus ameliorating disease severity. In contrast, when CNS cells are exposed directly to TFM-C, such as in the organotypic, astrocyte or microglia cultures, these cells may respond to Ca^{2+} perturbation differentially by either increasing or decreasing pro-inflammatory cytokine secretion. However, it remains to be determined whether TFM-C penetrates into the intact CNS following i.p. injection. If not, the main cellular mediators of its cytokine-modulating effects are likely to be the peripheral immune cells. This could explain why TFM-C failed to inhibit completely the development of EAE. In summary, we have described a new drug with potential beneficial effects for MS. The therapeutic niche covered by TFM-C may include beneficial effects in both innate and adaptive immunity, which is incompletely covered by current therapies [73]. In this sense, the therapy can be defined as acting in the interface between immunomodulation and neuroprotection. Thus, design of further non-coxib celecoxib analogues with improved activity profiles may be warranted.

Supporting Information

Figure S1. Effect of TFM-C on MHCII protein expression. Organotypic cultures were stimulated with LPS for 24h or pre-treated with TFM-C (50μM) for 2h and then stimulated with LPS/TFM-C for 24h. Immunofuorescence for Iba1 (red) and MHCII (green) was performed. White boxes show higher magnifications of merged images. Scale bar 50μm.
(TIF)

Figure S2. Effect of TFM-C on expression of genes belonging to Unfolded Protein Response (U), Ubiquitination (Ub) and Autophagy (A) pathways in HEK-293 cells and BV2 cells. A) HEK-293 cells were treated with TFM-C (50μM) for 12h and U, Ub and A PCR arrays were performed. The genes represented in the table are those with a fold increase higher than 2.5 compared with control samples